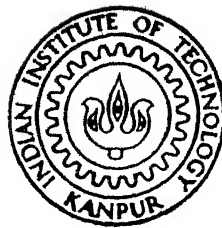# RECRYSTALLIZATION AND PRECIPITATION STUDIES
IN Al - 4.8% Mg AND 7075 ALUMINIUM ALLOY

by

Ms. UMA VERMA

DEPARTMENT OF METALLURGICAL ENGINEERING

INDIAN INSTITUTE OF TECHNOLOGY, KANPUR

FEBRUARY, 1988

RECRYSTALLIZATION AND PRECIPITATION STUDIES
IN Al - 4.8% Mg AND 7075 ALUMINIUM ALLOY

A Thesis Submitted
In Partial Fulfilment of the Requirements
tor the Degree of

MASTER OF TECHNOLOGY

by

Ms. UMA VERMA

to the

DEPARTMENT OF METALLURGICAL ENGINEERING

INDIAN INSTITUTE OF TECHNOLOGY, KANPUR

FEBRUARY, 1988
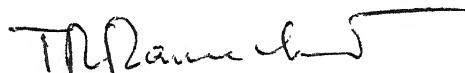
ME- 1980- M- VER- REC

CERTIFICATE

This is to certify that this work on "Recrystall-ization and Precipitation in Al-4.8 Percent Mg and 7075 Alloy" has been carried out by Miss Uma Verma under my supervision and has not been submitted elsewhere for a degree.

T. R. RAMACHANDRAN
Professor and Head
Department of Metallurgical Engineering
Indian Institute of Technology
Kanpur-208016

February, 1988.

ACKNOWLEDGEMENT

It is with immense pleasure and deep regards that I wish to express my inestimable debt of gratitude to Dr. T.R. Ramachandran, for his inspiring advice, keen interest, continued encouragement and invaluable guidance provided throughout the course of this study.

I take this opportunity to express my heartfelt gratitude to Mr. Rakesh and Ms. Uma Devi for their considerable help and enthusiastic aid throughout the course of present study. I wish to thank Mr. Rakesh Bhatnagar for his cooperation and patience with which he helped me in carrying out DSC experiments.

I convey my gratitude to all my friends who have helped me in the preparation of the thesis; directly or indirectly. Aradhana Srivastava, Abha and A.K. Singh have helped me in many ways. I am equally thankful to my friend and project partner Girish Kulkarni for his constant cooperation and honest advice.

Finally but not perfunctorily, I wish to thank Mr. R.N. Srivastava for his patience and deligence in typing and Mr. V.P. Gupta for making the figures for this manuscript.

CONTENTS

LIST OF TABLES

LIST OF FIGURES

ABSTRACT

Transmission electron microscopy has been used to characterize the microstructure in cold rolled and in two sta recrystallized (243°C for 2 min and 275°C for 2 min) Al-4.8 percent Mg alloy. The misorientation relationships between strained, recovered and recrystallized regions have been evaluated from selected area diffraction patterns.

Differential scanning calorimetric analysis has been used to characterize the solid state reaction undergoing in various tempers of 7075 alloy (5.6 Zn, 2.3 Mg, 1.6 Cu, 0.7 Fe, 0.5 Si, 0.3 Cr, 0.1 Ti and remaining Al) in the temperature range 30 to ~300°C. The tempers for present investigation are (i) solution treated, (ii) solution treated and 90 percent col rolled, (iii) T6, (iv) RRA and (v) T85. The steps involved in the heat treatments and importance of these tempers of 7075 aluminium are explained. The dissolution reaction occurring, have been elucidiated and expressed in terms of thermodynamic and kinetic parameters (peak temperature, dissolution enthalpy activation energy, activation entropy and activation free energy for (i) T6, (ii) RRA and (iii) T85 tempers. These parameters have been used to compare the estability of the preexisting matrix precipitates in these tempers. DSC analysis has also been applied to compare the precipitation in solution treated and solution treated plus cold rolled (90 percent) 7075 alloy.

TEM analysis of the Al-Mg alloy shows that deformatio

structure after cold rolling ($\varepsilon_T = 1.7$) consists of extensive

macroscopic shear bands and cell structure. Nucleation of

recrystallization has been observed both at shear bands and

at original high angle grain boundaries possibly by subgrain

coalescence mechanism. DSC analysis has shown that two

reactions which occur in the temperature range under consider-

ation are: dissolution of preexisting matrix precipitates and

formation of additional precipitates. These reactions can be

identified from the distinguishable peak temperatures. The

enthalpy for dissolution peak is directly proportional to

volume fraction of preexisting precipitates dissolving. The

relative stability of preexisting matrix precipitates in T6,

RRA and T85 is related primarily to activation entropy. It

is observed that this stability decreases as we go from RRA

to T85 and finally to T6 temper.

CHAPTER I

INTRODUCTION

1.1 Al-Mg System:

Aluminium-magnesium alloys combine a wide range of strength with good ductility. Although magnesium has substantial solubility in solid aluminium, binary Al-Mg alloys do not show appreciable precipitation hardening characteristics with concentrations below 7 percent magnesium. Magnesium, however, does provide the above mentioned properties through cold work in addition to excellent corrosion resistance and weldability. The Al-Mg binary phase diagram is shown in Figure 1.1 [1]. Magnesium is largely present in solid solution in wrought alloy, but it appears as eutectic Mg_2Al_3 in increasing amounts as Mg content increases. The composition of this phase is 37.3 percent Mg which is outside the limits of existence (34.8-37.1 percent Mg) whereas the formula Mg_5Al_8 (36 percent Mg) fits the composition and most of the structures given. Several structures have been proposed for Mg_5Al_8 as shown in Table 1.1 [2].

Table 1.1: Structures of Mg_5Al_8

Structure	Lattice parameters (10^{-10} m)	
	a	c
FCC	28.2 (Al end)	
FCC	28.2 (Mg end)	
FCC	12.419	
Hex	11.2-11.38	16.0-17.88

When magnesium content exceeds about 3.5 percent, Mg_5Al_8 precipitateson grain boundaries or within grains, but only slowly at ambient temperature which is accelerated if the alloys are in heavily worked condition. Chromium is a frequent additive in these alloys and may appear as a fine dispersoid of $Cr_2Mg_3Al_8$. When manganese is also present, iron rich phases become quite complex and $MnAl_6$, probably containing some chromium, appears as dispersoids. Small additions of chromium and manganese raise the recrystallization temperatures and tensile strength for a given Mg content.

Cold working of aluminium-magnesium alloys produce prominent deformation bands that are decorated by magnesium rich precipitates. Deformation morphology developed in cold rolled Al-Mg alloys has been studied by Lloyd et al. [3]. It is seen that slip is extremely inhomogeneous in these alloys and that strain is accommodated by a variety of means, including slip bands within grains, intense shear bands extending through a major portion of the thickness. Previous work [4] has shown that the β phase, Mg_2Al_3, can be precipitated to decorate the high strain region in these alloys. The early stages of recrystallization have been examined in a high purity Al-Mg alloy and in the commercial AA-5083 alloy by Lloyd [5]. In the essentially particle free Al-Mg alloy recrystallization nuclei are developed from subgrains which grow in regions of high deformation. In the commercial AA-5083 alloy recrystallization is mainly nucleated at constituent particles which have an associated deformation zone due to plastic incompatibility between the particle and matrix. While both the alloys
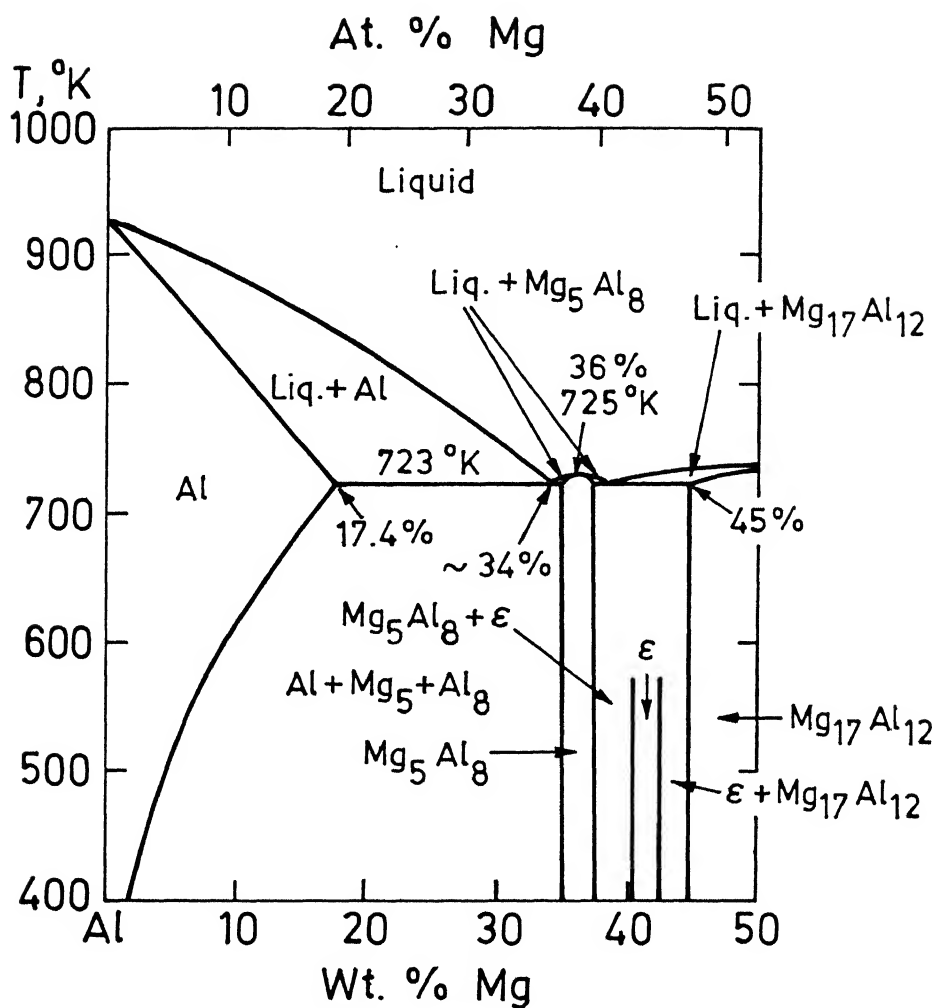
Fig. 1.1. The aluminium – magnesium equilibrium diagram

generate shear bands during cold rolling these are not a
major source of recrystallization nuclei. These aspects will
be discussed in Chapter II.

Many desirable characteristics of the aluminium-
magnesium alloys prompt usage in numerous areas where strengths
higher than those of pure aluminium are required. The higher
strengths and good welding qualities make them valuable in
transportation and structural fields, in the process industries,
and in military uses requiring good ballistic or cryogenic
properties. Decorative alloys with a wide range of strengths
and bright surface finish capabilities are also characteristic
of the aluminium-magnesium alloy system. This combination of
properties contributes significantly to the extensive uses of
these alloys. Important examples are the products for auto-
motive trim, architectural components, and other decorative
applications. The alloys used in this general field include
the 5 x 57 alloy.

1.2 Al-Zn-Mg-Cu System:

These alloys have received special attention because
it has long been realized that they have the greatest response
to age hardening of all aluminium alloys. However these alloys
proved to be unsuitable for structural use because of marked
susceptibility to stress corrosion cracking. Military needs
in the late 1930's and 1940's for aircraft alloys having high
strength/weight ratio eventually led to the introduction of
several Al-Zn-Mg-Cu alloys of which 7075 is perhaps the best
known. Since the present investigations are carried out on the

7075 aluminium alloy, the constitution, microstructure, metal-lurgy of heat treatment and properties of these alloys will be explained with reference to this alloy mainly.

The composition of 7075 alloy is given in Table 1.2.

Table 1.2: Composition of 7075

Alloy	Zn	Mg	Cu	Fe	Si	Cr	Mn	Ti
7075	5.6	2.5	1.6	0.7	0.5	0.3	0.3	0.2

The characteristics of the alloy depend upon the composition. Even a small amount of an element can cause a significant change in microstructure and thus properties. The effect and the purpose of all elements present in this alloy are discussed below.

Zinc and Magnesium:

Magnesium and zinc form $MgZn_2$, which produces a great response to heat treatment. Increase in $MgZn_2$ concentration increases the tensile and yield strengths. On the negative side, increasing additions of both zinc and magnesium affect the overall corrosion resistance of aluminium to the extent that close control over the microstructure, heat treatment, and composition are often necessary to maintain adequate resistance to stress corrosion attack.

Copper:

The addition of copper together with small but important amounts of chromium and manganese, in these alloys, results in the highest strength aluminium based alloys commercially available. The effect of copper is to increase the aging rate by increasing the degree of supersaturation and perhaps through nucleation of $CuMgAl_2$ phase. Copper also increases the quench sensitivity upon heat treatment. In general copper reduces the resistance to general corrosion of aluminium-zinc-magnesium alloys, but increases the resistance to stress corrosion cracking.

Chromium:

Small amounts of chromium, not exceeding 0.35 percent are added to control recrystallization and preserve the highly directional wrought grain structure. Chromium has a slow diffusion rate and forms fine dispersed phases. These dispersed phases inhibit nucleation and grain growth. Chromium in solid solution and as a finely dispersed phase increases the strengths of alloys slightly. The main drawback of chromium is the increase in quench sensitivity when the phase contributing to increase in hardness and strength tends to precipitate on pre-existing chromium phase particle.

Iron:

Iron is the most common impurity found in aluminium. It has a high solubility in molten aluminium and its solubility in solid state is very low (~0.4 percent) and therefore, most of iron present in aluminium over this amount appears as an

intermetallic second phase in combination with aluminium and often other elements. Iron reduces the grain size.

Manganese:

Manganese increases the strength and controls the grain structure. The effect of manganese is to increase recrystall-ization temperature and to promote the formation of fibrous structure upon hot working. As a dispersoid precipitate it is effective in slowing recovery and in preventing grain growth. Manganese precipitate increases quench sensitivity.

Silicon:

After iron, silicon is the highest impurity level. It forms Mg_2Si in these alloys.

Titanium:

Titanium is used primarily as a grain refiner. The phase diagram of Al-Zn-Mg-Cu is extremely complex and the results published do not give sufficient information for a complete and accurate picture of the system. A section of the phase diagram at $460^{\circ}C$ is shown in Figure 1.2 [6]. This is the usual temperature used for solution treatment of these alloys and it should be noted that some quaternary composition will not be single phase after such a treatment. The phases present in 7075 alloy have been identified by Ayer et al. [7]. The crystal structure and chemistry of submicron size particles have been studied using convergent beam electron diffraction and X-ray microanalysis respectively. The large particles could be
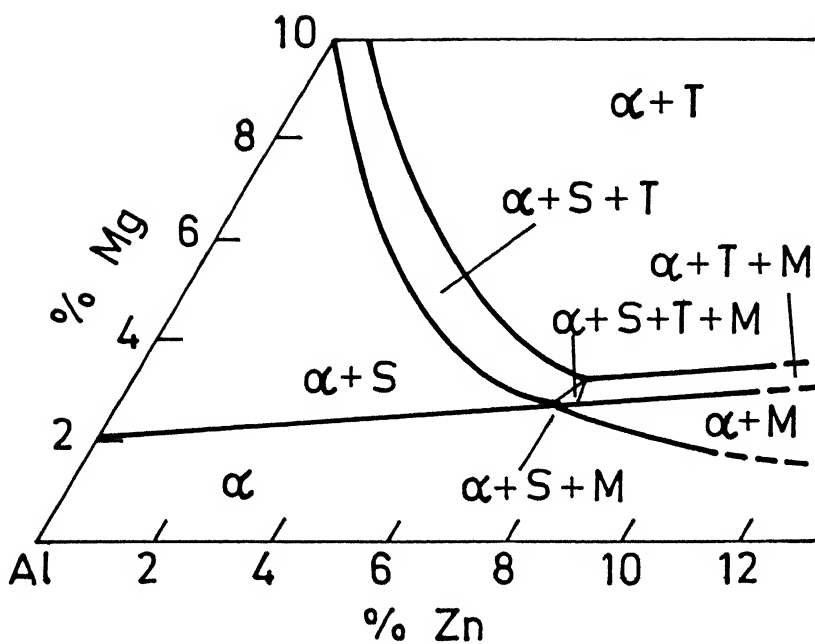
Fig. 1.2. Section of Al-Zn-Mg-Cu phase diagram (1.5% Cu) at 460°C

$S = Al_2CuMg$

$T = Al_6CuMg_4 + Al_{32}(Mg \cdot Zn)_{49}$

$M = MgZn_2 + AlCuMg$

Table 1.3:   Composition, structure and lattice parameter of various phases

Phases	Composition atomic percent ($\pm \sigma$)							Structure	Lattice parameters (nm)
	Al	Mg	Cu	Zn	Fe	Si	Others		
Al_7Cu_2Fe	68.3 (3.3)	–	20.6 (2.4)	0.8	9.6 (0.8)	–	0.8 Ni	Tetragonal	a = 0.6336 c = 1.487 $\alpha=\beta=\gamma=90°$
$(Al,Cu)_6(Fe,Cu)$	79.2 (2.7)	1.6 (0.4)	4.3 (0.4)	1.3 (0.4)	13.6 (1.2)	–	–	Orthorhombic	a = 0.6441 b = 0.7464 c = 0.8786 $\alpha=\beta=\gamma=90°$
Al_6Fe (modified)	73.2	–	3.5	0.4	16.8	3.3	2.0 Ni 0.5 Cr	Not possible to characterise fully due to sparse occurrence of this phase	–
Mg_2Si	2.0	66.4	–	–	–	31.6	–	Face centred cubic	a = 0.635 $\alpha=\beta=\gamma=90°$
α-$Al_{12}Fe_3Si$	74.0	1.8	2.1	0.4	14.2	5.9	1.2 Mn 0.4 Cr	–	–
SiO_2	–	–	–	–	–	40.0	60.0 oxygen	Amorphous	–
$Al_{18}Mg_3Cr_3$ (E-phase) $\Delta\gamma$	71.3 (0.9)	13.9 (1.0)	2.6 (0.2)	4.6 (0.2)	6.4 (0.8)	–	1.2 (0.6) Ti	–	–
$O\gamma$	71.5 (1.2)	13.7 (0.8)	2.6 (0.5)	4.5 (0.3)	6.5 (1.0)	–	1.2 (0.7) Ti	–	–

readily characterized in thin foils. The analysis of sub-micron dispersoid phases, however, could be carried out only on extraction residues to avoid interference of the surrounding matrix. The phase identified, their composition and lattice parameters are listed in Table 1.3 [7]. The other phases present in this alloy, as can be seen from the section of phase diagram in Figure 1.2, are $Al_2CuMg(S)$, Al_6CuMg_4, $Al_{32}(Mg,Zn)_{49}(T)$, $MgZn_2$ and $AlCuMg(M)$. The structure, morphology and orientation relationships with the matrix, for $MgZn_2$ and $Al_{32}(Mg,Zn)_{49}$ precipitates, will be summarized later in Table 1.5.

1.2.1 Precipitation in Al-Zn-Mg-Cu alloys:

Precipitation processes constitute a primary means of manipulating microstructure and properties in both metals and non-metals. Aluminium alloys show a marked response to precipitation hardening. The basic requirement for an alloy to be amenable to age hardening, is decrease in solid solution of one or more of alloying elements with decreasing temperature. Heat treatment normally involves:

(i)   Solution treatment at a relatively high temperature within the single phase region,

(ii) Rapid cooling or quenching, usually to room temperature, to obtain a supersaturated solid solution of these elements in aluminium, and

(iii) Controlled decomposition of the SSSS to form a finely dispersed precipitate (coherent or semi-coherent with the matrix), usually by ageing for convenient time at one and sometimes two intermediate temperatures.

Solution treatment is actually heating the product to suitable temperature, holding at that temperature for time long enough to dissolve the alloying elements. The temperature must be limited to a safe level below maximum to avoid consequences of overheating and partial melting. The time required for solution treatment depends on the type of product, alloy and thickness in so far as it influences preexisting microstructure. These factors establish the proportions of the solutes that are in or out of solution and the size and distribution of precipitated phase.

Quenching is in many ways a critical step in the sequence of heat treating operations. The objective of quenching is to preserve the solid solution formed at the solution treatment temperature by rapidly cooling to some lower temperature and also to maintain a certain minimum number of vacant sites to assist in promoting the low temperature diffusion required for zone formation.

Most alloys exhibit property changes at room temperature after quenching. This is called "natural ageing" and may start immediately after quenching or after an incubation period. The rates vary from one alloy to another so that approach to a stable condition may require only a few days or several years. 7075-W (water quenched) and aged for 25 years at room temperature is seen to consist of GP zones throughout the structure having an average diameter of 1.2 nm and approximate density 4×10^{18} zones per cm^3. During this natural ageing, yield strength is observed to increase from 150 MPa to 465 MPa.

Precipitation can be accentuated in these alloys and their strength, further increased by heating above room temperature. This operation is referred to as artificial ageing. In certain alloys, considerable additional increase in strength can be obtained by imposing controlled amounts of cold work on the product after quenching and this extra strength is attributed to strain hardening. Precipitation is further accentuated if cold working is followed by precipitation heat treating. Aluminium Association has described temper designation applicable to heat-treatable alloys, depending upon the combination and sequences of cold working and precipitation heat treatments. The basis temper designation are: T_1, T_2, T_3 ... T_{10} etc. and the designations involving additional digit are assigned to stress releived tempers of wrought products for e.g., T_{-51} etc.

For different alloys, these tempers have different importance because of different microstructure and effects on properties. The tempers T_6, T_{651}, T_{7351}, RRA and T_{85} are employed with 7075 aluminium to achieve improvement in strength and stress corrosion cracking resistance. The tempers, their corresponding effect on microstructure, mechanical and corrosion properties have been reviewed in detail in Chapter II. The improvement of strength and corrosion resistance depends upon the nature of precipitates and their distribution in the matrix. In Al-Zn-Mg-Cu alloys of commercial interest the ageing sequence is:

Supersaturated Solid Solution $\rightarrow$ GP zones $\rightarrow$ η' $\rightarrow$ η (MgZn)

$\rightarrow$ $T((Al,Zn)_{49}Mg_{32})$.

(a) GP Zones:

The ageing of rapidly quenched Al-Zn-Mg-Cu alloys from room temperature to relatively low temperatures ($\sim$160°C) is accompanied by the generation of GP zones having an approximately spherical shape. With increasing ageing time, GP zones increase in size which has been evaluated by Adler et al. [8] and results are summarized here in Table 1.4. Naess [9] studied

Table 1.4: Microstructural characteristics of precipitates in T_6 temper of 7075 aluminium

Condition	Matrix precipitate
Solution treated at 490 $\pm$ 5°C for 2 hrs. water quenched + aged	
120°C – 8 h	fine GP zones ($\leq$50 $\overset{\circ}{A}$)
120°C – 16 h	spherical GP zones ($\leq$75 $\overset{\circ}{A}$)
120°C – 24 h	spherical GP zones ($\leq$75 $\overset{\circ}{A}$) + η' (125 $\overset{\circ}{A}$)
120°C – 48 h	spherical GP zones ($\leq$75 $\overset{\circ}{A}$) + η' (200 to 300 $\overset{\circ}{A}$)

zone formation, by using divergent beam X-ray diffraction techniques and detected first an increase in the lattice parameter of the matrix and then a decrease on prolonged ageing and these results were explained in terms of a hypothesis originally proposed by Guinier, that two types of zones exist: one containing pure or nearly pure zinc and the other ordered magnesium and zinc atoms. Thomas and Nutting [10] used thin film

transmission electron microscopy to study zone formation is an Al-7 weight percent Zn-2.4 weight percent magnesium alloy and reported spherical zones formation as the first stage of ageing at both 120 and 160°C. Embury and Nicholson [11] detected spherical zones about 35 $\overset{o}{A}$ in diameter after ageing an Al-5.9 weight percent zinc-2.9 weight percent magnesium alloy at 135°C for 20 minutes. At an ageing temperature of 180°C a similar structure was observed after 10 minutes ageing but the particles had a more angular morphology than the GP zones formed at 135°C. It has been reported that GP zones were coherent with the matrix at the early stages of ageing and that as ageing proceeded the spherical zones were replaced by an ordered hexagonal structure with orientation relationship

$$(0001)_{Hex} \mid\mid (11\bar{1})_{\alpha} \; ; \quad [10\bar{1}0]_{Hex} \mid\mid [1\bar{1}0]_{\alpha}$$

These particles were proposed to be precursors of hexagonal η'.

(b) η':

Mondolfo et al. [12] postulated the existence of the transitional η' phase from studies of Al-6.2 weight percent zinc-2.1 weight percent magnesium alloy aged at 200°C. Even prolonged ageing above room temperature transforms the GP zones in alloys with relatively high zinc-magnesium ratios into η'. Mondolfo et al. proposed that η' was hexagonal, a = 4.96 $\overset{o}{A}$, c = 8.68 $\overset{o}{A}$, with the orientation relationship with the matrix of

$$(0001)_{\eta'} \mid\mid (111)_{\alpha} \; ; \quad [11\bar{2}0]_{\eta'} \mid\mid [112]_{\alpha}$$

Gjonnes et al. [13] and others reported that η' was the precursor of stable η phase.

$\underline{\eta}$:

The presence of a hexagonal η (MgZn$_2$) phase with a = 5.21 $\overset{\circ}{A}$ and c = 8.60 $\overset{\circ}{A}$ is well established. It has a number of orientation relationships with the matrix which are summarized in Table 1.5.

Table 1.5: Morphology of η and its orientation relationship with Al matrix

Type	Morphology	Orientation relationship
1	6 or 8 sided plates on {100}$_\alpha$	$(10\bar{1}0)_\eta$ ‖ $(001)_\alpha$; $(001)_\eta$ ‖ $(110)_\alpha$
2	Hexagonal plates on {111}$_\alpha$	$(0001)_\eta$ ‖ $(1\bar{1}\bar{1})_\alpha$; $(10\bar{1}0)_\eta$ ‖ $(110)_\alpha$
3	Hexagonal plates on {100}	$(0001)_\eta$ ‖ $(1\bar{1}\bar{1})_\alpha$; $(11\bar{2}0)_\eta$ ‖ $(110)_\alpha$
4	Rods or plates on {111}$_\alpha$	$(0001)_\eta$ ‖ $(110)_\alpha$; $(\bar{1}2\bar{1}0)_\eta$ ‖ $(1\bar{1}\bar{1})_\alpha$
5	Rods or plates on {111}$_\alpha$	$(\bar{1}2\bar{1}0)_\eta$ ‖ $(1\bar{1}\bar{1})_\alpha$; $(30\bar{3}2)_\eta$ ‖ $(110)_\alpha$
6	Rods along <$1\bar{1}2$>$_\alpha$	$(\bar{1}2\bar{1}0)_\eta$ ‖ $(001)_\alpha$; $(0001)_\eta$ ‖ $(110)_\alpha$

$\underline{T}$:

The T phase ((Al,Zn)$_{49}$Mg$_{32}$) is cubic with a = 14.16 $\overset{\circ}{A}$. Schmalzried and Gerold [14] reported the presence of the phase in samples aged above 190°C with the orientation relationship

$$(100)_T \text{ II } (112)_\alpha \; ; \quad [001]_T \text{ II } [110]_\alpha$$

Embury and Nicholson [11] found that ageing at $300^\circ C$ produced
T phase which was irregular in morphology and had a bcc struc-
ture with a $= 14.16 \overset{O}{A}$.

1.2.2 Hardening mechanism:

During the initial stages, the principal change is a
redistribution of solute atoms within the solid solution
lattice to form clusters of GP zones that are considerable
enriched in solute. This local segregation of solute atoms
produces a distortion of the lattice planes both within the
zones and extending for several atom layers into the matrix
with an increase in the number or density of zones, the degree
of disturbance of the regularity and periodicity of the lattice
increases. The strengthening effect of the zones results from
the additional interference with the motion of dislocations
when they cut the GP zones. This may be because of chemical
strengthening (production of a new particle matrix interface)
and the increase in stress required to move a dislocation
through a region distorted by coherency stresses. The progre-
ssive strength increase during natural ageing has been attri-
buted to an increase in the size of the GP zones in some
systems and to increase in their number in others.

The transition precipitates η' have specific crystallo-
graphic orientation relationships with the solid solution,
such that the two phases remain coherent on certain planes by
adaptation of the matrix through local elastic strain. The
strengthening effects of these semicoherent transition

structures are related to the impedence to dislocation motion provided by the presence of lattice strains and precipitate particles. The strength continues to increase as the size of these precipitates increases, as long as the dislocations continue to cut the precipitates. When these transition phase, η', changes to η on further ageing, there is loss of coherency strain and strengthening effects are caused by the stress required to cause dislocation to loop around rather than cut the precipitates. Strength progressively decreases with growth of equilibrium phase particles and an increase in interparticle spacing.

1.2.3 Kinetics of precipitation:

The rate at which precipitation reactions occur depends on the respective diffusion rates in addition to solubilities and alloying contents. Diffusion of the substitutional solid solution forming elements, as well as self-diffusion, is believed to occur primarily by a vacancy exchange mechanism. Vacancies have a particularly significant role in the formation of GP zones. Precise measurement of electrical resistivities and relative changes in density and lattice conditions with temperature have been used to ascertain an equilibrium concentration of vacancies in aluminium that varies with temperature. The increased low temperature solute mobility required to account for the high rates of zone formation was explained by a vacancy-assisted diffusion mechanism, made possible by the retention of a non-equilibrium high vacancy concentration at the low temperature. In addition to fundamental role of vacancies

several specific interactions between vacancies and various solute atoms influence ageing kinetics and make the effect of trace elements important. Magnesium appears to play a special role in this process. Because of its large atomic diameter, magnesium vacancy complexes are readily formed and make retention of excess vacancies during quenching easier.

1.2.4 Nucleation:

The formation of zones can occur in an essentially continuous crystal lattice by a process of homogeneous nucleation. Several investigations provide evidence that critical vacancy concentration is required for this process and that a nucleation model involving vacancy-solute atoms clusters is consistent with certain effects of solution temperature and quenching rate. The nucleation of new phase is greatly influenced by discontinuities in the lattice such as grain boundaries, subgrain boundaries, dislocations, and interphase boundaries. Because these sites are locations of greater disorder and higher energy than the solid solution matrix, they nucleate either transition or equilibrium precipitates. The solute that precipitates in this uncontrolled manner during quench is unavailable for subsequent precipitation either at room temperature or elevated temperature, so precipitation during quench can effect the development of properties. The effect on strength of precipitating during the quench onto grain boundaries, subgrain boundaries, and scattered particles on the order of 0.5 μm or larger is generally negligible. The effect

of precipitation onto the fine dispersoid particles (<0.1 μm) formed by high temperature precipitation at an earlier stage in the processing, however, can be large when the rate of cooling is not rapid enough.

CHAPTER II

LITERATURE REVIEW

2.1   Second Phase Particles:

Commercially used alloys are solid solution alloys
and more often two phase alloys. The second phase particles in
two phase alloys are commonly classified into three types:
constituents, dispersoids and fine strengthening precipitates.
The constituent phases are relatively large (2 to 5 μm) and
consist of insoluble and partially soluble intermetallic comp-
ounds. These compounds primarily form during casting, as a
result of interaction of the alloying elements with the
impurity elements such as Fe and Si. $Al_{12}Fe_3Si$, Al_6Fe, Al_3Fe,
Al_6Mn etc. are common examples of constituents in Al-alloys.
Dispersoids, which are also intermetallic compounds, are rela-
tively smaller in size (0.2 to 1 μm) and typically contain
elements such as Mg, Cu, Zn, Cr and Zr. These elements are
intentionally added for either strengthening or to act as nuclea-
tion sites for the recrystallization. Recently an attempt was
made to introduce the dispersoids in Al-Zn-Mg-Cu 7075 alloy by
suitable over ageing treatments [15]. Two steps involved in
this process were (i) solution treatment and (ii) overaging
treatment. The alloy solution treated at 480 $\pm$ 2^{O}C for two
hours and quenched in water contained a dispersion of insoluble
particles which were approximately 0.1 μm in diameter and
homogeneously dispersed. To produce a dispersion of particles
sufficiently large to act as nucleation sites for recrystallizing

grains the overaging treatment was carried out at $400^{\circ}C$ for
8 hours. The dispersion of precipitates of approximately 1 μm
diameter was obtained. Composition analysis of these particles
by STEM showed that majority of particles contained Al, Zn,
Mg and Cu. X-ray diffraction confirmed the presence of
$MgZn_2$ + AlCuMg [15].

The strengthening precipitates form during hot rolling
and ageing treatments in an extremely fine and homogeneous
dispersion.

2.2   Deformation Structure:

When an alloy is cold-rolled its deformation structure
depends upon whether the alloy is single-phase alloy or two-
phase alloy. We shall consider deformation structure of both
of these alloys one by one.

2.3   Solid Solution Alloy:

The deformation structure of solid solution alloy is
similar to that of pure metal which may consist of cells, tran-
sition bands and shear bands. Their characteristics are
discussed below.

2.3.1   Cell structure:

The region inside the grains of deformed alloys are
broken up into units which are described as arrangements of
slightly misoriented "crystal domains" referred to as cells.
The cell structure forms as a result of ability of screw dislo-
cations to cross slip out of their original slip planes and

arrange themselves in a very localized region which form walls on relatively strain-free cells.

The cell size and sharpness depends upon the following factors:

a)   Stacking fault energy,

b)   Composition of the alloy,

c)   Deformation temperature, and

d)   The strain rate.

a) Stacking fault energy: The sharpness of the cell walls formed during plastic deformation depends upon the stacking fault energy. A stacking fault is bounded by partial dislocations, the width of this fault is inversely proportional to the stacking fault energy. Metals with high stacking fault energy for e.g. Al produce narrow stacking faults during deformation. So in such cases hindrence to cross slip is less and the cell structure formed is clearly defined.

b) Composition of the alloy: Solid solution elements reduce the cell size in deformed metals because increase in solute content leads to a decrease in stacking fault energy which in turn increases the stacking fault width so the cell structure formed is not well defined. It is also because of decrease in dislocation density and the stored energy for any given strain.

c) Deformation temperature: The dislocation density increases with decrease in deformation temperature which causes reduction of both the stacking fault energy and the dislocation slip distance.   So the tendency for cell formation becomes less

pronounced. Keh [16] and Warrington [17] have shown that the cell size increases as the deformation temperature is raised above room temperature.

d) The strain rate: The effect of increase in strain rate has been found to be similar to that of reduction in deformation temperature i.e. dislocation density and stored energy are increased and thus tendency to form sharply defined cells is diminished.

The average cell diameter is of the order 1 to 3 μm though it changes from one grain to another because each grain in polycrystal deforms by a different amount depending upon its orientation and constraints imposed on it by its neighbours.

2.3.2 Transition bands:

In moderately deformed metals, misorientation develop within individual grains at features which are described as 'transition bands'. These deformation bands separate two regions of an original grain that have rotated in two different ways towards alternative end orientations during deformation.

The formation of transition bands [18, 19, 20, 21] has been observed in α-Fe, Al and single crystal Al deformed in various ways. In these studies it was found that the extent and severity of transition banding increased with strain, increased grain size and the change from rolling to uniaxial compression.

2.3.3 Shear bands:

These are the bands of localized shear strain which originate due to any form of work softening in alloys so that strain concentrate into these bands instead of being dispersed more homogeneously by work hardening. These bands are best seen on longitudinal sections of rolled material and develop after strains greater than about 60 percent reduction in thickness. The shear bands are a few micrometers in thickness and cut across grain boundaries.

The shear bands have been observed by Lloyd et al. [22] in a high purity Al-4.5 percent Mg alloy. It has been found that the homogeneous dislocation structure formed at low strains becomes unstable at high strains with the bands being area of local softening due to dislocation rearrangement and annihilation. Another factor contributing to the inhomogeneity of deformation is the response of some of the individual grains. Majority of grains increasingly elongate with strain, but there are many which essentially retain their original shape. Such grains behave in the matrix as if they are rigid inclusions. Thus flow pattern is being disturbed around them to accommodate the plastic strain mismatch between themselves and the heavily deforming matrix.

In the early stages of deformation ($\approx$20 percent reduction), there is only one set of deformation lines per grain but as the deformation increases the length and breadth of the shear bands increase and bands become more wavy. These bands tend to cluster and extend across many grain diameters to form macroscopic shear bands.

Shear bands have also been observed two phase alloys which will be described later.

2.4 Two Phase Alloys:

Deformation structure of two phase alloys consist of deformation zone and shear band.

2.4.1 Deformation zone:

The cold working of such alloys result in higher dislocation density around the large particle than in the surrounding matrix due to local misfit strains. These regions of higher dislocation density are commonly known as "deformation zones". A well developed substructure is present in these zones. The appearance of deformation zone in Al-alloys has been studied by Humphreys (1977) [22] and Herbst and Huber (1978) [23].

2.4.2 Shear bands:

The alloy like Al-Cu and Cu-Cr which have suitable precipitate structures, show shear banding. The precipitates in these alloys are cut and damaged by dislocations during slip which allows strain to concentrate into these bands instead of being dispersed more homogeneously by work hardening. Klein (1970) [24], Hornbogen and ZumGahr (1975) [25], and Lea et al. (1979) [26] have studied shear banding in the alloys like Al-Cu and Cu-Cr.

2.5 Recovery and Recrystallization in Al-alloys:

2.5.1 Recovery:

Under favourable conditions, a cold worked metal returns to unworked state or annealed state, and stored energy provides the driving force for the process involved. Two processes involved are recovery and recrystallization. Recovery includes all those changes which do not involve sweeping of the deformed structure by migrating high angle boundaries. During recovery process the stored energy is annealed out during progressive heating in terms of following processes:

(i)   Elimination of dipoles,

(ii)   the mutual annihilation of dislocations of opposite sign, and finally

(iii)   the rearrangement of the remaining dislocations into more stable arrays possessing lower value of strain energy.

2.5.2 Recrystallization:

Recrystallization is the process in which new grains are nucleated and growth of new grains occurs at the expense of the deformed metal. At this stage the new grains will impinge on each other and the process is then complete.

Cahn [27] and Doherty [28] have reviewed the various mechanisms which have been proposed to account for the formation of recrystallization nuclei.

(a) <u>Polygonization</u>:   Cahn [29] and Beck [30] independently, proposed that polygonization could produce dislocation-free

subgrains, one of which would become viable nucleus.

(b)   Subgrain coalescence by rotation: Hu [31, 32] formulated subgrain coalescence theory which explains that dislocations gradually move out from disappearing subgrain boundary into other boundaries around the subgrains.

This probably requires some dislocation climb along the disappearing boundary, a rotation of the subgrain itself, and movement of some of the atoms situated immediately around the relevant boundaries. The possibility of subgrain rotation, during recrystallization, has been thoroughly examined by Li [33]. He summarised his finding as "A subgrain can rotate naturally in a direction in which low angle boundaries decrease their angles of misfit to allow high angle boundaries to increase their angle of misfit".

The energy for subgrain coalescence comes from the difference between the high energy of a dislocation in a low angle boundary and the lower energy associated with a high-angle boundary.

(c)   The geometric coalescence model: Nielsen postulated the coalescence of two neighbouring subgrains having similar, but not necessarily identical orientations. Such coalescence is said to occur by the movement of atoms from outside to inside the coalescing pair of subgrains. There is no basic increase in the misorientation between the coalesced subgrain and its neighbour. It is, therefore, difficult to see how geometric coalescence alone can fully cause formation of a viable recrystallization nucleus for which presence of high angle

boundary in the deformation zone is must.

The process of geometric coalescence is likely to be involved in nucleation as a part of rotation coalescence.

(d) Nucleation by grain boundary bulging: This mechanism was first postulated by Beck and Sperry. It is assumed that (i) the boundary is capable of high mobility due to a large misorientation between the two grains which it separates and (ii) there is significant strain difference in two grains. In these circumstances the migration of boundaries starts from the boundary of grain containing large subgrains and migrate away from this grain into heavily strained grain which contains smaller subgrains. The basic driving force is the difference in stored energy values for such two grains.

2.6 Recrystallization in Single Phase Alloys:

Criterion for nucleation of recrystallization: the nucleus must obtain high angle boundaries. Nucleation site for recrystallization, can be grain boundaries, shear band and transition band.

2.6.1 Nucleation at the grain boundaries:

In single phase alloys, grain boundaries and triple lines are regions where high angle boundaries already exist so that criterion for the nucleation of recrystallization is satisfied. Nucleation occurs by subgrain coalescence by rotation and strain induced grain boundary migration mechanisms as there is a difference in dislocation density across a grain boundary and due to which there is difference, also, in subcell

size across the grain boundary in cold worked material. An
extension of this process will eventually result in a small
grain surrounded by a high angle boundary of large size
enough to grow progressively in the matrix. Bellier and
Doherty [18] found that in coarse grained aluminium alloys
compressed 20 percent, only across prior grain boundaries did
the metal have local misorientations of more than 20°. Nucle-
ation then occurred solely by nuclei on one side of a grain
boundary growing into the adjacent deformed grains, the process
of strain induced boundary migration. Inokuti and Doherty [19]
reported similar observations on coarse grained iron rolled 40
percent. It seems that in the absence of other types of
lattice curvature the only sites for nucleation will be pre-
existing grain boundaries.

2.6.2 Nucleation at transition bands:

The materials which contain transition bands in their
deformed structure, do not always show preferential nucleation
at the transition bands. Doherty (1978) [34], Bellier and
Doherty [18] showed that when there were small misorientations
(less than 20°) across the transition bands in Al compressed
10 or 20 percent, although there was some enhanced subgrain
growth at the transition bands, these enlarged subgrains grew
so slowly that they failed to become nuclei before grain
boundary nucleated recrystallization swept through the material.
Only with large misorientations, for example, in coarse grained
Al compressed 40 percent, did nucleation occur readily at the
transition bands.

2.6.3 Nucleation at shear bands:

As the shear bands produce large local lattice rotation, these bands are common sites for nucleation of recrystallization. In some cases it has been observed that while nucleation occurred readily in the shear band but the subsequent growth of nucleii into the surrounding deformed metal occurred more slowly.

Annealing of the alloys containing shear bands cause appearance of new grains. Some of these grains are aligned along the direction of the shear bands which is consistent with shear band nucleation.

Apart from formation of new grains at shear bands, disappearance of most shear bands has been observed during annealing. There is no shear band when recrystallization is complete. Nucleation at shear bands has been observed by Adcock (1922) [35], Grewen et al. (1977) [36], Duggan et al. (1978b) [37], Noda et al. (1978) [38], and Huber and Hatherby (1979) [39].

2.6.4 Effect of solute atoms on recrystallization in solid solution alloys:

It has been observed that recrystallization process is retarded as the solute content of a solid-solution alloy is increased. More experimental work has been carried out on Al-based solid solutions than on any other individual metal solvent because of its extreme sensitivity to the effect of impurities. Recrystallization temperature of 'super-purity' and 99.99 percent purity Al differed by about 100°C. The

investigators interpreted the observed recrystallization delay in terms of solute/grain boundary and solute/dislocation interactions which, it was proposed, increased the activation energy necessary for grain boundary movement. Boundary movement is affected by the following factors:

(1)   the nature of solute distribution around a moving boundary,

(2)   the interaction forces between boundary and solute atoms, and

(3)   the diffusion of solute in a potential field adjacent to the boundary.

2.7 Recrystallization in Two Phase Alloys:

Recrystallization has been divided the recrystallization process into three stages [40] :

(i)   Formation of a nucleus from pre-existing subgrains,

(ii)   recrystallization of the deformation zone, and

(iii)   growth of recrystallization beyond the deformation zone. The particles affect the recrystallization rate and recrystallized grain size through their size and spacing.

2.7.1 Effect on recrystallization rate:

(a)   Coarse particles, widely spaced: A dispersion of particles with size greater than 0.5 μm and the spacing ≥ 2.5 μm, causes an intense deformation zone around itself and acts as preferential site for nucleation of new grains during recrystallization.

(b)   Fine particles, closely spaced: Such dispersion
        retard the recrystallization process because of lack
        of local misorientation.

(c)   Fine particles, widely spaced: It would have limited
        effect on nucleation and this is supported by the
        observation of Jones et al. (1979) [41].

2.7.2 Effect on recrystallized grain size:

(a)   Large particles increase the recrystallized grain
        density by increasing the density of nucleation sites.

(b)   Small particles have been found to decrease recrystal-
        lization density in some cases by interfering with
        nucleation of recrystallizing grains, thus decreasing
        the overall nucleation rate.

2.8 Precipitation in 7075 Aluminium Alloy:

2.8.1 Introduction

        7075 aluminium alloys are of commercial significance
because they develop the highest strength of all aluminium
alloys. However, these alloys are highly susceptible to stress
corrosion cracking which put a limitation on its applications.
The strength of this alloy is associated mainly with matrix
containing GP zones while stress corrosion cracking is cont-
rolled by grain boundary precipitates, their interparticle
distances and precipitate free zone (PFZ) width. This indicates
that improvement in mechanical and corrosion properties should
be possible by designing combination of matrix and grain

boundary structure. Some of these aspects will be discussed in detail in this section.

A number of heat treatment tempers such as T4, T6, T651, T85 and two step aging are used to form GP zones in the matrix of the 7075 alloys. T73 and T7351 are employed with 7075 to achieve stress corrosion cracking resistance but these tempers result in lower strength. Recently a treatment known as Retrogression and Reaging (RRA) has been employed with 7075 to obtain stress corrosion cracking resistance equivalent to the T73 temper together with T6 strength levels. The heat treatment steps involved in developing these tempers for 7075 aluminium alloy, the microstructure and effect on mechanical and corrosion properties are discussed in detail in this section.

2.8.2 Heat treatment:

Heat treatment conditions for various tempers are given in Table 2.1.

2.8.3 Effect of heat treatment on microstructure of 7075 aluminium

The effect of above mentioned tempers on the matrix and grain boundary structure are tabulated in Table 2.2 [42].

It can be seen from Tables 2.1 and 2.2 that

(i) 1 percent stretching between quenching and ageing causes slight increase in η' size which affect the strength.

(ii) Two stage T7351 treatment is preferred because exposure at lower temperature allows the formation of a

Table 2.1:   Heat treatment condition for various tempers

Temper	Heat treatment condition[⊕]
Conventional temper	
T_4	Naturally aged
T_6 [•]	Aged at $120^O C$ for 8 h, 16 h or 24 h
T_6 [‡]	Aged at $120^O C$ for 8 h, 16 h or 24 h
T_8	Cold worked to a suitable extent and aged at $120^O C$ for 24 hours e.g. cold worked to 5 percent and aged at $120^O C$ for 24 hours referred as T85
Modified temper	
Two step ageing	Aging at $100^O C$ for 4 h and then at $160^O C$ for 8 h
T_{651}	1 percent stretching followed by ageing at $120^O C$ for 8, 16 or 24 h
T_{7351}	1 percent stretching, aged at $175^O C$ for 9 h
T_{7351}	1 percent stretching, aged at $120^O C$ for 24 h and then at $175^O C$ for 9 h
Retrogression (applied on T_6 temper)	Ageing at $120^O C$ for 24 h to obtain T_6 temper, heated at $200^O C$ for a short interval ranging 5 min to 60 min
Retrogression and Reaging	Retrogression same as above then ageing at $120^O C$ for 24 hours

⊕ Solution treatment carried out at 490 $\pm$ $5^O C$ for 24 hours and quenching in water except in T_6 [‡] for which liquid nitrogen quenching is used.

Table 2.2: Effect of heat treatment on microstructure of 7075

| Temper | Matrix precipitate | Grain boundary precipitate | | | PFZ width, A° |
		Small density	Size A°	Large size A°	
T4 (25 years)	Fine GP zones (~12 Å)	-	-	-	-
T6 (8 h)	Fine GP zones (≤50 Å)	390	140±60	(1000 to 3000)	300
T6 (16 h)	Spherical GP zones (≤75 Å)	340	190±90	(1000 to 3000)	300
T6 (24 h)	Spherical GP zones (≤75 Å) + η' (125 Å)	300	270±120	(2000 to 4000)	300
T6‡ (8 h)	Very fine GP zones (≤30 Å)	370	175±100	3300 ± 1000	1000
T6‡ (16 h)	Fine GP zones (≤50 Å)	250	220±110	3300 ± 1000	1000
T6‡ (24 h)	Spherical GP zones (≤75 Å)	210	275±105	4400 ± 2200	1000
T651 (8 h)	Fine GP zones (≤50 Å)	660	130±60	1000 to 3000	200
T651 (16 h)	Spherical GP zones (≤75 Å)	320	230±60	1000 to 3000	200
T651 (24 h)	Spherical GP zones (~150 Å) + η' (~150 Å)	260	310±150	1000 to 3000	200
T7351 (120°C for 24 h + 175°C for 9 h)	η' (100 to 300 Å) + η(400 to 800 Å)	60	900±2800	4800 ± 1400	900

large number of GP zones which are stable at higher
temperature. The zones transform to intermediate η'
precipitate and finally to equilibrium $\eta(MgZn_2)$ phase
during overaging. If the first stage i.e. heating at
$120^{\circ}C$ for 24 h is eliminated then because of GP zone
reversion and insufficient nuclei for the formation of
fine dispersion of η. First stage of T7351 can be
replaced by extended natural ageing which also permits
GP zones to grow to a size that resist reversion during
second stage. Such GP zones also transform to η' and
finally to equilibrium η phase but due to extended time
for this process, it is not practical. One percent
stretching does not affect the matrix structure but
grain boundary precipitate growth appears to be enhanced.

(iii)   Two step ageing treatment: The microstructure deve-
loped during ageing depends upon the delay between
quenching and ageing. In 7075 aluminium, delays of 4
to 30 h have more detrimental effect on properties than
longer delays. It can be due to decrease in degree of
supersaturation existing in the quenched state and
reversion of GP zones during artificial ageing. The
effects of natural ageing interval for 7075-T6 temper
are eliminated by use of two step ageing treatment.
First step at $100^{\circ}C$ permits GP zones to grow to a size
that does not dissolve when the temperature is raised.

(iv)   Retrogression: During retrogression a slight increase
in matrix precipitate size has been observed and is
shown in Figure 2.1 [43] upto 5 min. of retrogression
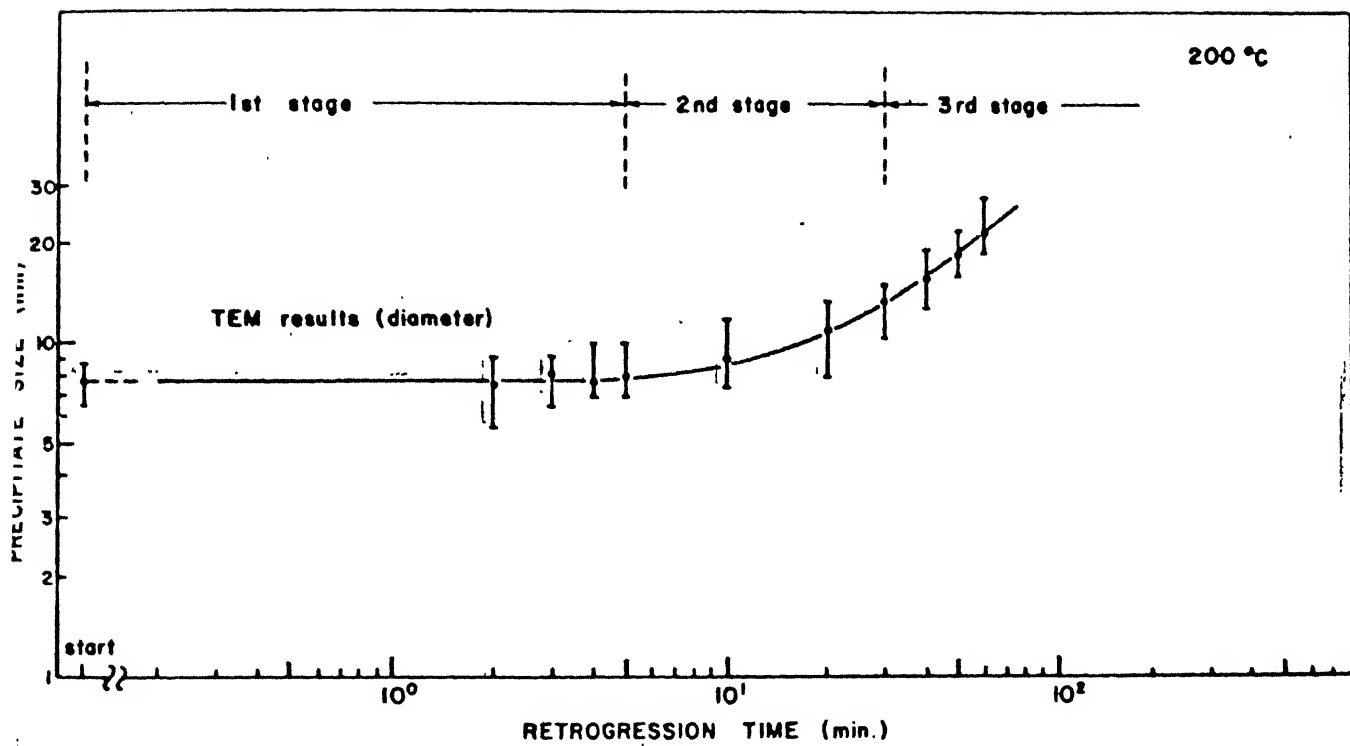
Fig. 2.1   Changes in precipitate size during retrogression.

there is no significant change in precipitate size.
After 5 min., there is a gradual increase in precipitate
size upto 30 min. after which there is increase in rate
of precipitate growth. Another microstructural change
during retrogression is the increase of total volume
fraction of η' and η as shown in Table 2.3.

(v)   Retrogression and reageing: After a short time of
five minutes of retrogression at 200°C followed by
reageing, the total volume fraction of η' and η preci-
pitates increased over both T6 and corresponding
retrogressed condition. The details are shown in
Table 2.3 [43]. Also there is a slight increase in
precipitate size compared to that of retrogressed
material. Under certain conditions, this treatment
increases volume fraction of semicoherent η' precipi-
tates without significantly coarsening them.

2.8.4 Effect of heat treatment on mechanical properties:

Typical mechanical properties of this alloy for
T6, T651, T73 and T7351 are given in Table 2.4 [44].

Table 2.3: Total increase in volume fraction of η' and η during retrogression and RRA

Heat treatment condition	Volume fraction
T6	0.029
Retrogressed-5 minutes	0.031
Retrogressed-5 minutes and reaged	0.047
Retrogressed-30 minutes	0.071
Retrogressed-60 minutes	0.120

Table 2.4: Typical mechanical properties of 7075 aluminium for various tempers

Temper	Tensile ultimate strength MPa	Tensile yield strength MPa	Elonga-tion in 50 mm (percentage)	Hard-ness BHN	Shear strength MPa	Fatigue limit MPa
T6, T651	570	505	11	150	330	160
T73, T7351	505	435	13	–	–	150

Retrogression: During retrogression the change in yield strength vs. retrogression time can be divided into three stages: the initial rapid drop in strength, the subsequent increase in strength giving rise to a secondary peak and the last stage where strength begins to drop again. This is shown in Figure 2.2 [43].

Retrogression and Reageing: The reageing treatment carried out on retrogressed materials allowed a maximum increase in yield strength of about 5 percent with respect to that of the T6 condition. Even after long times of retrogression, the reageing treatment could still improve yield strength by upto 4 percent compared to retrogressed specimens. This is also shown in Figure 2.2.

The changes in strength during various treatments can be related to the microstructure.

The increase in yield strength, tensile strength and hardness are related to the growth of GP zones during ageing. Strengthening mechanism has already been described in Chapter I. Ductility of the temper depends upon PFZ width. At the same level of strength material with a wider PFZ undergoes greater localized deformation and has lower hardness than narrower PFZ material. Since T6 or T651 temper the matrix structure is primarily GP zones whereas T7351 temper consists of η' and η and no GP zones. This explains the reason why T6 or T651 temper has strength greater than that for T7351. Wider PFZ of T7351 as compared to that of T651 is responsible for higher ductility and lower hardness of T7351 than that of T651.
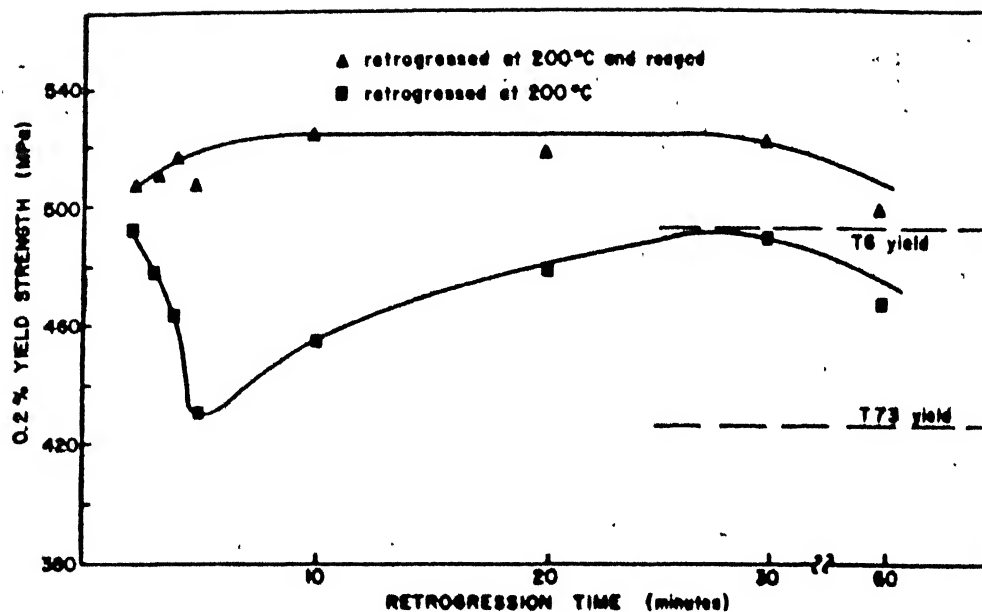
Fig. 2.2 Changes in yield strength during retrogression at 200°C and after retrogression plus reageing treatment.

Initial decrease in strength is due to the dissolution
of the coherent GP zones. During the GP zones reversion or
dissolution process, the growth of the pre-existing η' and the
nucleation of new η' particles on the remaining GP zones could
occur simultaneously. TEM investigation of first stage of
retrogression showed that there was no noticeable change in
size and distribution of η' precipitates from the T6 condition
until minimum of strength vs. retrogression time curve has
reached. This suggest that GP zone reversion and not η' growth
dominate during this stage of the process. Deiasi and Adler
[45] found from combination of DSC and hot stage TEM that GP
zone dissolution and the formation and growth of η' precipitate
occur simultaneously at temperatures upto $217^{\circ}C$. However GP
zone dissolution was found to be predominant. This implies
that only dissolution of GP zones was responsible for the
initial loss of strength.

During second stage of retrogression, there occurs an
increase in strength which was attributed to an increase in
volume fraction of η' and η. Some workers [46, 47, 48] have
shown that η' would provide the predominant contribution to
strength at the retrogression temperature. Thus it was sugg-
ested by Dahn et al. [43] that the total increase in volume
fraction of precipitates was mostly due to increase in the
amount of η'. Although an increase in size of precipitate
was also observed but this increase was not large enough to
dominate volume fraction effects. The precipitate growth rate
increases in the third stage noticeably when there is drop in

strength due to overageing. It is felt that growth of incoherent   is predominant at this stage.

The RRA can simply be considered as a two step ageing process; the first step involves retrogression and the second step represents the reageing treatment. In the initial step, retrogression causes the partial dissolution of pre-existing GP zones. However, this dissolution, furthermore, enriches the matrix in Zn and Mg, which in turn promotes the nucleation and growth of η' phase. In the second reageing process both GP zones and η' precipitate can nucleate and grow. However, the nucleation and growth of η' should be dominant over nucleation and growth of GP zones, following the suggestions of Ryum [48] and Inoue et al. [46]. Also some increase in volume fraction of precipitates over both the original T6 condition and corresponding retrogressed condition Kovac et al. [49] found that the η' contribution to strengthening through Orowan mechanism was larger than that of the coherent GP zones which are sheared by dislocations. The high density and homogeneous distribution of the η' particles observed and high strength of alloy are in agreement with the observations of Kovacs et al. [49].

2.9 Differential Scanning Calorimetric Analysis of Al-alloy:

2.9.1 DSC analysis to study recrystallization:

Differential scanning calorimetric (DSC) has been used to examine many solid state reactions occurring in aluminium alloys. While many microstructural features that are analyzed by DSC can also be observed by metallographic methods, DSC has the advantages of

(i)   analyzing comparatively large volume of material,

(ii)   quantitative data output (heat effects, activation

       energy and activation entropy),

(iii) minimal time for study, and

(iv)   ease of sample preparation.

Aluminium alloys are well suited for DSC studies because of their good thermal conductivities are relatively low melting points. DSC analysis has been used to study recrystallization in 3003 Al-Mn alloy (Mn 1.07, Fe 0.63, Cu 0.15, Si 0.24, traces of Mg, Cr, Zn and Ti and remaining Al). Samples were subjected to a variety of treatments: (i) solution treated, (ii) solution treated and 80 percent cold rolled and (iii) precipitation treated and 80 percent cold rolled. These result in microstructure consisting of supersaturated solid solution (SSSS), deformed SSSS and Mn rich particles in deformed Al-matrix respectively. DSC thermograms obtained for each of these sample for a heating rate of 5^OC/min are shown in Figure 2.3 [50].

DSC thermogram for sample (i) shows one peak in temperature range 325 to 550°C which is due to precipitation. For the second sample, four peaks (i) a low broad peak between about 100 and 250°C which is due to slight precipitation of Mn on the dislocation structure and, possibly, some minor rearrangement of dislocation, (ii) a small but sharp peak at 291°C which is due to rapid precipitation of Mn on the initial dislocation structure, (iii) a broad peak at 334°C due to recovery processes and (iv) a sharp peak at 398°C due to recrystallization. At 480°C recrystallization is complete.

Further heating causes dissolution of Mn precipitates. DSC thermogram for sample (iii) which contains Mn rich precipitates and is strain hardened shows three peaks (i) a low broad peak between about 275 and 310°C with maximum approximately at 290°C is mainly due to recovery, (ii) a sharp peak at 333°C representing recrystallization and (iii) a broad peak at 470°C. At 470°C recrystallization is complete and further heating causes dissolution of Mn precipitates.

2.9.2 DSC analysis to study precipitation:

A number of investigators have also examined the basic precipitation processes in Al-Cu alloy [51-54], Al-Mg [55, 56], Al-Mg-Si [57-62] and Al-Zn-Mg [63-68] alloys. These age hardening alloys involve relatively fast diffusing atomic species and have large enthalpies of reaction, making them well suited for analysis by DSC. Solid state reactions accompanying heating of the highest strength (T651) and overaged T7351 tempers of 7075 aluminium alloy have been studied by Deiasi and Adler [45]. Calorimetric measurements were made using a Dupont 900 Thermal Analyzer containing a differential Scanning Calorimeter (DSC) plug-in-module at a heating rate of 10°C/min over a range from room temperature to 480°C. Dry nitrogen (1 x 10^{-4} m^3/min) was passed through calorimeter to minimize oxidation.

It has already been explained in this chapter that microstructure of T651 (24 h) of 7075 aluminium consists primarily of GP zones with a small concentration (5 percent) of the semicoherent transitional phase, η' whereas microstructure of

T7351 consists of a mixture of η' and the stable, incoherent η phase. DSC technique has been used to characterize the solid state reactions accompanying the dissolution of these matrix precipitates, as well as the formation of additional precipitates. The dissolution of each matrix phase i.e. GP zones, η' and η, could be characterized by a distinguishable dissolution temperature, dissolution enthalpy, activation energy activation entropy and free energy of activation. The values of activation energy and activation entropy for the dissolution of initial matrix precipitate indicated that the relative stability of the matrix precipitates is primarily influenced by activation entropy rather than the energy term. This investigation provides a basis for the use of DSC analysis in rapid, quantitative identification of the matrix microstructure of 7075 aluminium alloys. Hot stage TEM used in conjunction with DSC helped to follow the reactions accompanying heating. Typical results obtained by DSC analysis, plotted as differential heat capacity (ΔC_p) vs. temperature curves are shown in Figure 2.4 [45].

For T651 temper, DSC curve contained endothermic region from 113 to 217°C, exothermic doublet between 217 to 271°C and another endotherm between 271 to 448°C.

For T7351 temper an endotherm from 164 to 245°C and another endotherm from 245 to 442°C have been observed. Combination of TEM and DSC results, could identify the reactions occurring in these regions. These are shown in Table 2.5 [45].

These regions were analyzed to characterize reaction temperature, enthalpy, and kinetics of the overriding reactions
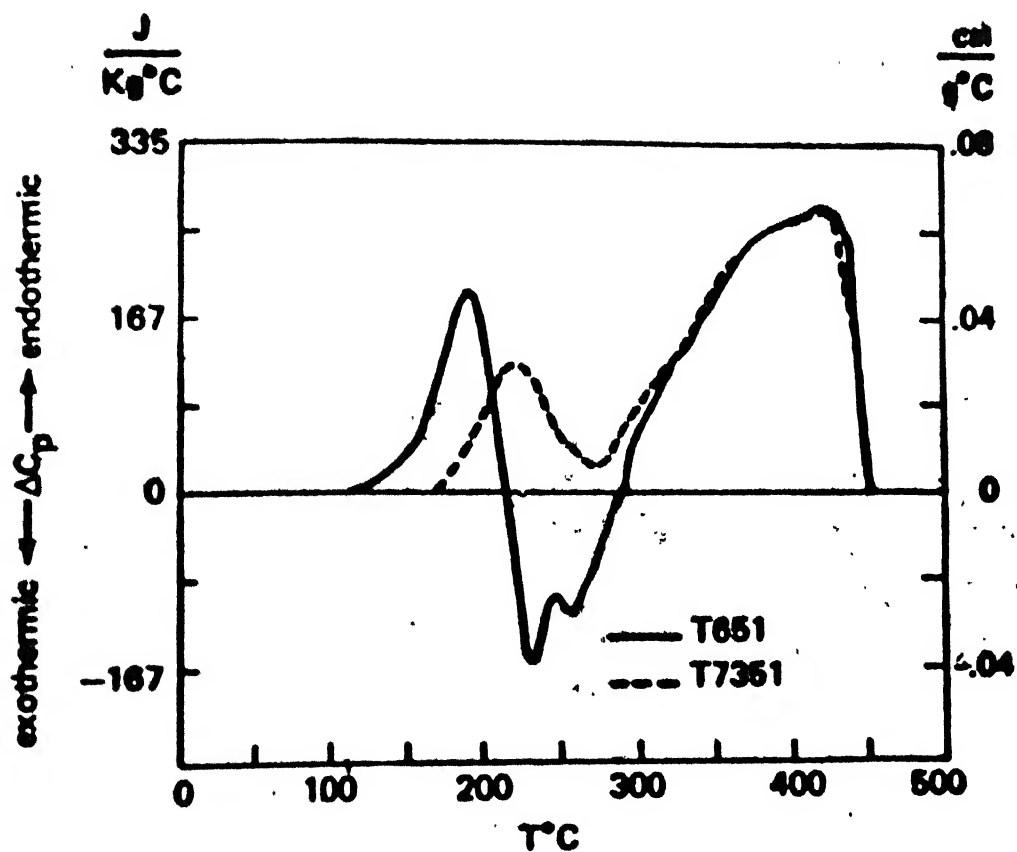
Fig. 2.4   The heat capacity changes during heating of T651
and T7351 tempers of 7075.

Table 2.5: Reactions occurring in regions of DSC analysis
for 7075 aluminium alloy

Temper	Region	Temperature range °C	Predominant reaction	Other reaction
T651	1	113 to 217	GP zone dissolution	η' formation η' growth η' dissolution
	2	217 to 271	-	η' formation η formation η' dissolution η dissolution
	3	271 to 448	η dissolution	-
T7351	1	164 to 245	η' dissolution	η formation η growth
	2	245 to 442	η dissolution	-

corresponding to specific temperature regions. The peak temp-
erature, T_p, for a specific endotherm or exotherm in a measure
of the temperature at which the reaction is occurring at a
maximum rate. The area of specific endothermic or exothermic
region of the ΔC_p vs. T curves corresponds to the enthalpy
associated with the reaction occurring over the indicated
temperature range. For example, the area under endothermic
curve is a measure of the heat of reaction associated with
precipitate dissolution. For a specific precipitate this
value ΔH_R, is proportional to the volume fraction of the preci-
pitate undergoing dissolution. This can be expressed by the
equation:

$$\Delta H_R \;=\; \frac{\Delta H_p}{M_p} \;=\; \frac{\rho_p}{\rho_s}\, V_f$$

where

ΔH_p = molar heat of dissolution of precipitate,

M_p = molecular weight of precipitate,

ρ_p = density of precipitate,

ρ_s = density of sample, and

V_f = precipitate volume fraction.

The kinetics associated with the dissolution in these regions were also evaluated from the DSC curve. The rate constant for these dissolution reactions were calculated by using the following relationship

$$K_r \;=\; Q\,\frac{\Delta C_p}{(A - a_t)}$$

where

K_r = specific reaction rate constant,

Q = a constant heating rate,

ΔC_p = differential heat capacity,

A = total area under the dissolution peak, and

a_t = the area under the peak to time t.

Values of K_r as a function of temperature were obtained by computer programmed stepwise integration of the dissolution peaks. Absolute reaction rate theory was applied to the dissolution reactions for each temper under consideration, and the activation energy, E_a, and activation entropy, 'ΔS' were determined. These results of kinetic analysis are shown in Table 2.6 [45].

Table 2.6:   DSC characteristics of 7075 aluminium alloy

Temper	Region	Peak temperature $^{\circ}C$	Temperature range for kinetic analysis $^{\circ}C$	ΔH_R J/kg	E_a kJ/mole	ΔS J/mole $^{\circ}C$
T651	1	190 ± 2	130 to 203	7360 ± 920	107.4 ± 6.7	-72.7 ± 15.9
	2	229 ± 2	–	3930 ± 2720	–	
		255 ± 1				
	3	389 ± 9	290 to 412	26580 ± 4310	66.5 ± 4.2	-216.5 ± 5.4
T7351	1	218 ± 2	175 to 244	6230 ± 630	86.1 ± 7.1	-136.3 ± 10
	2	390 ± 16	264 to 415	29690 ± 5480	63.1 ± 5.4	-221.5 ± 7.5

The initial portion of the regions were eliminated because of small errors in the measurement of 'a_t' would be manifested as large errors in the rate constants. The final portions of region were eliminated because of possible thermal lag of the instrument in returning to the base line. For T651 temper the kinetics for exothermic region were not evaluated because of overlapping reactions occurring over a narrow temperature range. A knowledge of the microstructural changes associated with specific temperature regions (Table 2.5) would be helpful in explaining the significance of thermodynamic and kinetic data obtained for both tempers. The peak dissolution temperature for first endotherm of T7351 is $28^{\circ}C$ higher than that for

region 1 of T651 which is apparent because heating of T651
temper alloy involves dissolution of GP zones and that of
T7351 temper alloy involves dissolution of η' phase. Comparable
value of peak temperature for second endotherm is due to diss-
olution of stable phase in both tempers. Higher values of
heat of dissolution for first endotherm for T651 temper than
for T7351 is due to higher volume fraction of GP zones observed
in the matrix of T651 temper than of η' phase in the matrix of
T7351.

The kinetics of dissolution of GP zones, η' and η
could be easily distinguished by comparing activation entropy
changes for their dissolution. The entropy change associated
with the formation of the activated complex is the smallest
for GP zones dissolution and largest for dissolution of η.
The highest entropy for η dissolution indicates the lowest
activation site probability.

CHAPTER III

EXPERIMENTAL PROCEDURES

3.1   Summary of Investigations:

The present investigations have been concentrated mainly
on the following.

3.1.1   Study on Al-Mg alloy:

(a)   Deformation structure of an Al-Mg alloy,

(b)   Recrystallization behaviour of the same alloy,
using transmission electron microscopy.

3.1.2   Study on Al-Zn-Mg-Cu alloy:

(a)   The differential scanning calorimetric analysis to
study solid state reactions from $30^\circ C$ to $350^\circ C$ for a number of
tempers (i) solution treated, (ii) solution treated and 90 per-
cent cold rolled, (iii) T6, (iv) RRA and (v) T85 of 7075 alumin-
ium alloy.

(b)   The possible interaction between the precipitation
and recrystallization of solution treatment followed by 90 per-
cent deformation.

3.2   Material Studied:

3.2.1   Al-Mg alloy:

Composition of alloy used for investigations is 4.8 per-
cent Mg and remaining Al.

3.2.2 Al-Zn-Mg-Cu alloy:

7075 aluminium alloy (5.6 Zn, 2.5 Mg, 1.6 Cu, 0.7 Fe, 0.5 Si, 0.3 Cr, 0.2 Mn, 0.1 Ti and remaining Al) has been used for present investigations. The starting material was a cylindrical bar with 11 cm diameter and 8 cm length.

3.3 Preliminary Treatments:

3.3.1 Preliminary treatment for Al-Mg alloy:

(a) Al-4.8 percent Mg was rolled to a true strain, ε_t = 1.7.

(b) Deformed alloy is recrystallized at two stage: (i) at 243°C for 2 min and then (ii) at 275°C for 2 min, in a salt bath with composition 45 percent KNO_3-55 percent $NaNO_2$. This low melting point salt bath was chosen to permit rapid heating of the samples.

3.3.2 Preliminary treatment for Al-Zn-Mg-Cu alloy:

Five rectangular pieces of 5 x 3 x 0.4 cm^3 size were cut from the cylindrical bar and all were solution treated at 490 $\pm$ 5°C for 2 hours. Solution treatment was carried out in salt bath in a tubular furnace. The temperature of the furnace was maintained at the required value and controlled to an accuracy of $\pm$5°C using Aplab temperature controller. The furnace was calibrated using Chromel-Alumel thermocouple and milivoltmeter. The salt bath was 50 percent NaCN and 50 percent KCN. All the five samples were subsequently quenched in cold water.

Sample II was immediately cold rolled to 90 percent whereas Samples III to V were given T6, RRR and T85 treatments under the same conditions as explained in Chapter II.

3.4 Sample Preparation:

3.4.1 Sample preparation for TEM analysis:

The electron microscope specimens were prepared from the experimental material in two different stages. The first of these was mechanical thinning. Pieces of size 1.5 x 1.0 x 0.04 cm^3 were cut from rolled strips. These were thinned down to a thickness of 0.1 mm by polishing on 3/0 followed by polishing on 4/0. Discs of 3.0 mm diameter were punched out with a standard Fischione punch. In the second stage, disc samples were thinned by a standard twin-jet electropolishing technique. The electrolyte was a mixture of two parts methanol and one part nitric acid used at a temperature of less than $-15^{\circ}C$ at an applied voltage of 10 V. As soon as the central section of specimen was thinned and light through fiber optics on the light source side of the specimen reached the fiber optics of the opposite side of specimen through it, the photocell activated audible and visual alarm. The specimen holder was immediately removed from the electrolyte and rinsed in distilled water. The specimen was removed from specimen holder and rinsed in distilled water, methanol, and distilled water filled in four successive beakers. The samples were dried and preserved in petridishes for electronmicroscopic observations.

3.4.2 Sample preparation for DSC analysis:

DSC samples were cut from each of five pieces and ground to the form of disc of approximately 5.0 mm diameter and ∿1.0 mm thickness. DSC analysis were performed on a Dupont 900 Thermal Analyzer equipped with a DSC cell. The test information from Dupont thermal analyzer is sent to the data recorder through the recorder jacks located on the rear panel of the Dupont Thermal Analyzer.

CHAPTER   IV

RESULTS AND DISCUSSION

4.1 Introduction

As stated earlier electron microscopic studies were used to understand the deformation morphology developed in cold rolled (ε_T = 1.7) Al-4.8 percent Mg alloy. Also a two stage recrystallization (i) 243°C for 2 min and (ii) 275°C for 2 min after cold rolling of the same alloy. In addition to this Differential Scanning Calorimetry (DSC) studies were carried out on Al-Zn-Mg-Cu 7075 aluminium alloy to characterize the matrix precipitates and compare the stability of various tempers (i) solution treated, (ii) solution treated and 90 percent cold rolled, (iii) T6, (iv) RRA and (v) T85. The results obtained and their significance are discussed in the following sections.

4.2 Transmission Electron Microscopic Analysis:

In TEM, the deformation structure consists of shear bands of high dislocation density superimposed on a background of relatively uniform density (Figure 4.1) and substructure with dislocation tangles. These shear bands are usually along the traces of the (III) slip planes. On recrystallization many small grains have formed. Some of these grains are aligned along the direction of shear bands but this is not a predominant mechanism. Most of shear bands have disappeared (Figure 4.2). A number of subgrains
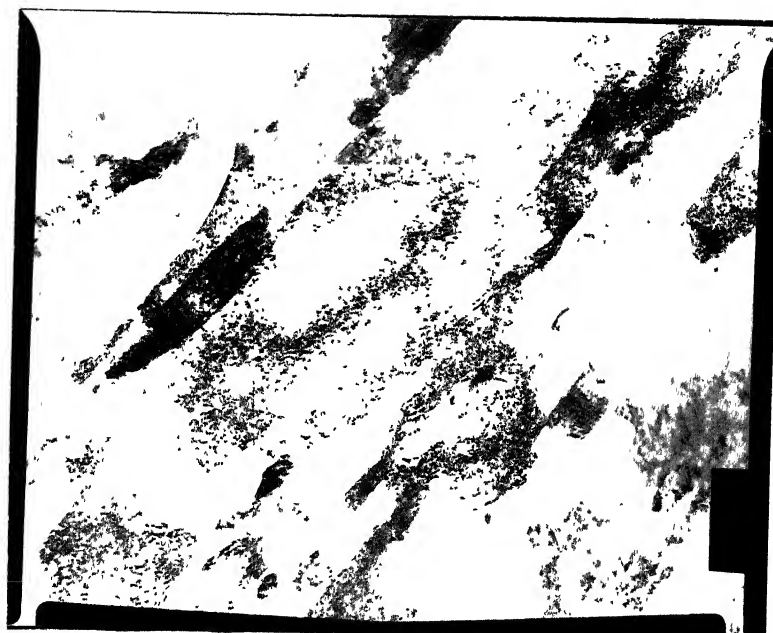
0.85μm

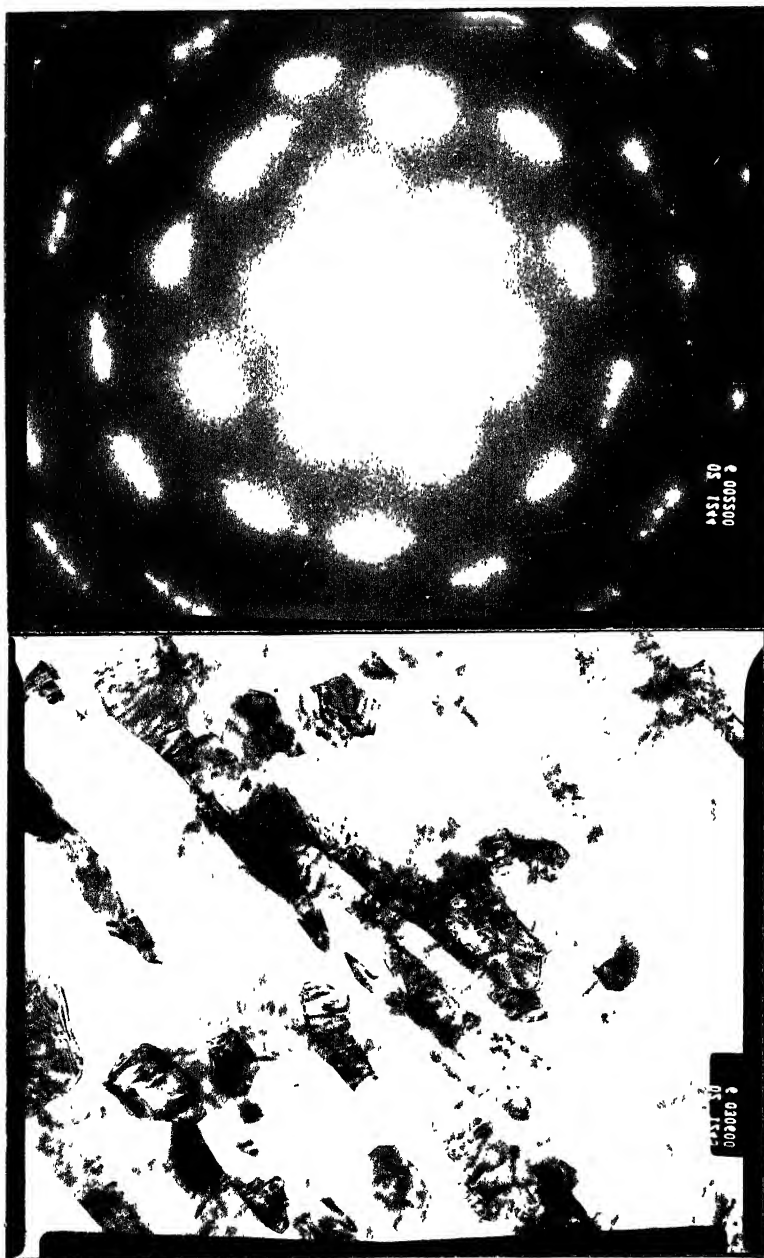Fig. 4.1   Shear bands in cold rolled Al–Mg alloy.

Fig. 4.2 Recrystallization near the shear bands.

are also observed in recovered region. Quite a few of
these have been marked A, B, C, D, E and F in Figure 4.3
which is a montage from recovered regions. Another micro-
graph in Figure 4.4 is again a montage shows a region marked
A where recrystallization has just started. This region shows
that recrystallization is occurring by subgrain coalescence.
This mechanism has already been explained in Chapter II. The
other important feature of this montage are recrystallized
grain marked B. The distribution of orientation between
different regions marked B, C, D and E in this montage were
evaluated from selected area diffraction patterns obtained
from corresponding region. Selected area diffraction (SAD)
patterns from B, C, D and E are shown in Figure 4.5. The spot
patterns were analyzed by using standard ratio method.

The distances 'R' from the central spot to three
diffraction spots which form a parallelogram, the ratios of
these 'R' values corresponds to ratio of d values. The
measured ratios are correlated with the actual d_{hkl} values
obtained from tables of interplanar spacings. The angle bet-
ween the spots is measured. One of the closest spots is
arbitrarily indexed with a particular (hkl) value and by
knowing the possible (hkl) indices for the other two spots
and the angles between the first spot, origin and the two
other diffraction spots, exact indices can be assigned. If
$(h_1k_1l_1)$ and $(h_2k_2l_2)$ are the indices of the spots and $(h_1k_1l_1)$
is positioned anticlockwise around the centre relative to
$(h_2k_2l_2)$ then the indices UVW of the diffraction antiparallel
to the electron beam direction are given by
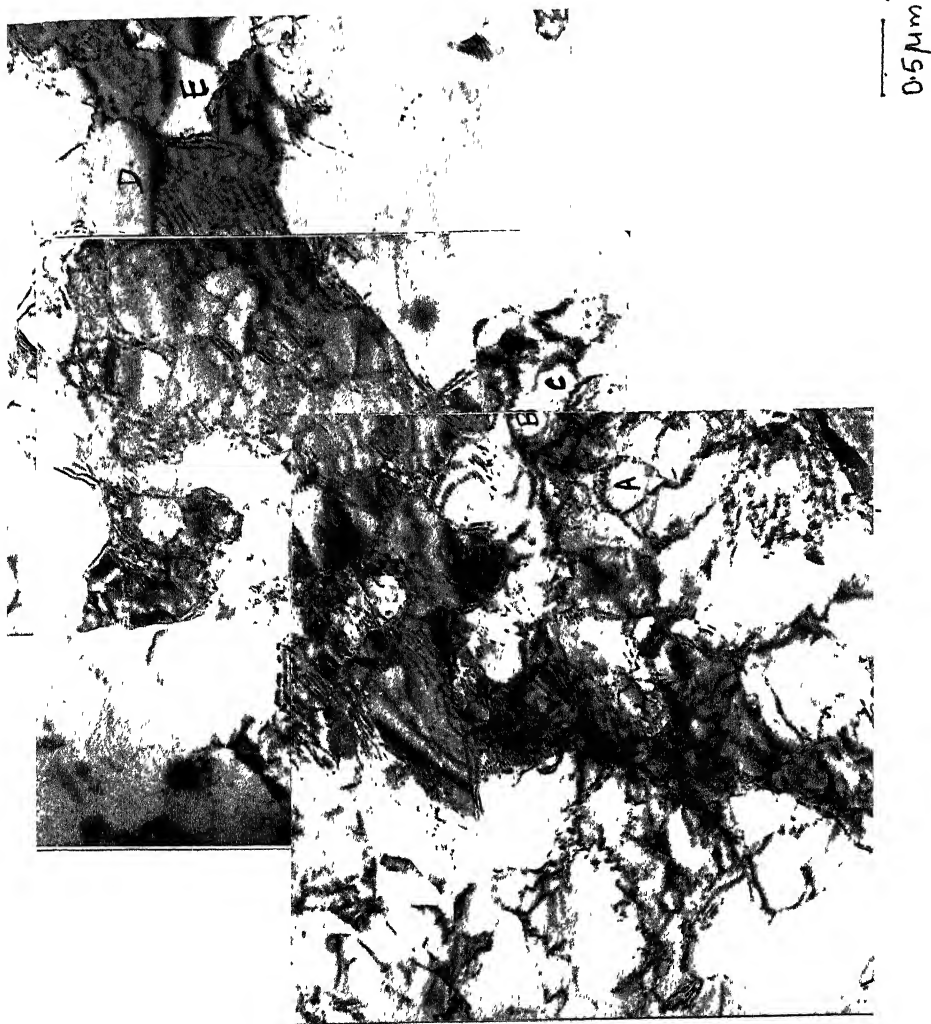
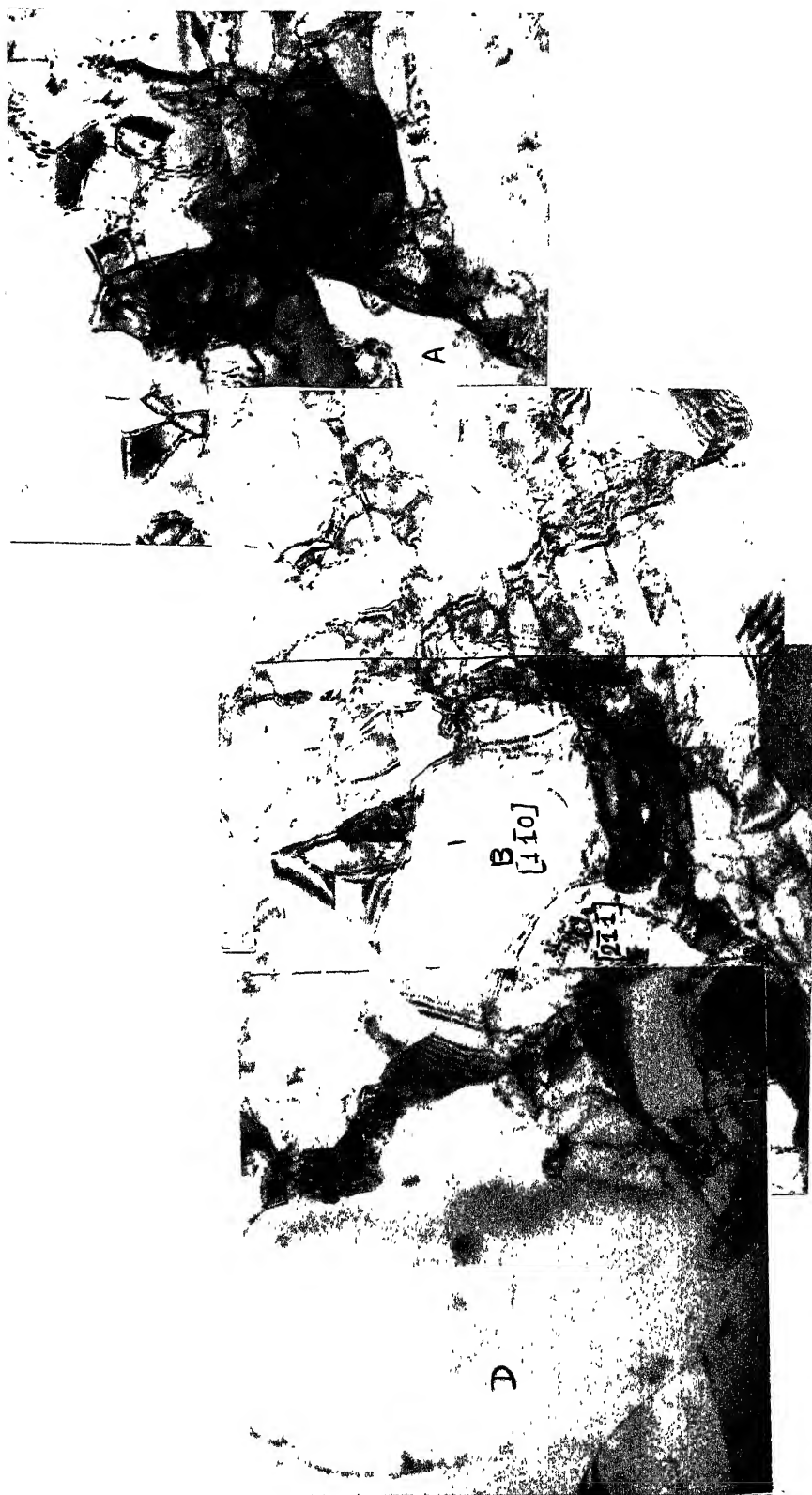Fig. 4.3   Subgrain structure after two stage annealing.

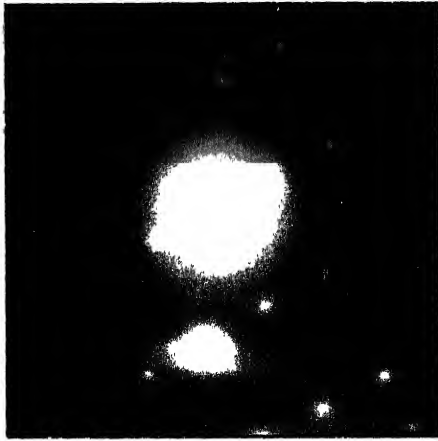Fig. 4.4   Both subgrains and recrystallized grain present after two stage annealing.

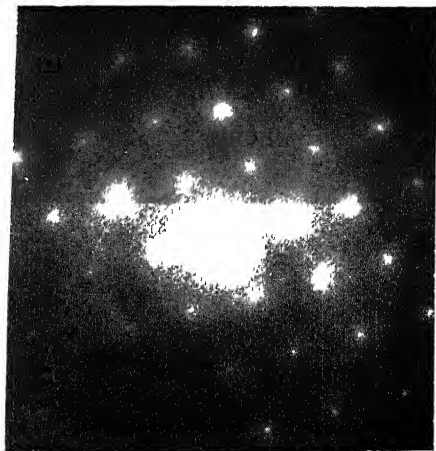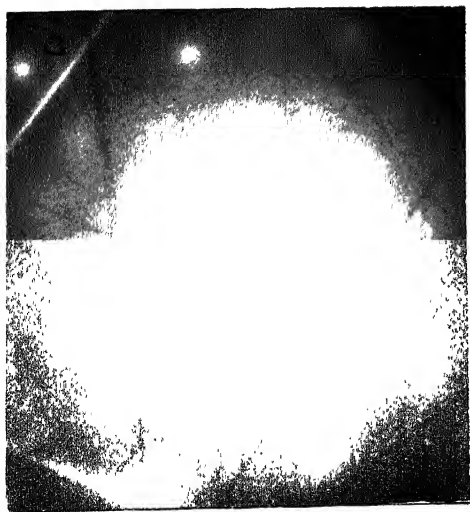Fig. 4.5   Diffraction pattern from different regions of Fig. 4.4.

62

Fig. 4.6   Diffraction pattern from different regions of Fig. 4.4.

$$U = k_1 l_2 - k_2 l_1$$

$$V = l_1 h_2 - l_2 h_2$$

$$\text{and} \quad W = h_1 k_2 - h_2 k_1$$

The results obtained on solving these patterns are given.

B

The values of R are 0.86, 0.9 and 1.0 cms. The angle measured are 110° between R_1 and R_3 and 55.5° between R_1 and R_2. The ratios R_1/R_2 and R_1/R_3 are evaluated; these are 0.966 and 0.935 respectively comparing these ratios with ratios of d values, indices of possible planes are found to be (111), ($\bar{1}\bar{1}$1) and (002). The angle between (111) and ($\bar{1}\bar{1}$1) is given by relationship $\cos^{-1}(\frac{-1}{\sqrt{9}})$ i.e. 109.47° which is close to observed angle. The angle between (111) and (002) is given by $\cos^{-1} \frac{2}{\sqrt{3 \times 4}}$ i.e. 54.7 which fits very well with the measured angle. The vector ($\bar{1}\bar{1}$1) is anticlockwise with respect to 111, the indices UVW of the direction antiparallel to the electron beam are given by,

$$\begin{array}{cc} \bar{1} \\ 1 \end{array} \Big| \begin{array}{cc} \bar{1} & 1 \\ 1 & 1 \end{array} \qquad \begin{array}{cc} \bar{1} & \bar{1} \\ 1 & 1 \end{array} \Big| \begin{array}{c} 1 \\ 1 \end{array}$$

$$U = \bar{2}, \quad V = 2, \quad W = 0$$

The electron beam direction is therefore $[\bar{1}10]$.

C

The diffraction pattern is taken from slightly recovered region in the neighbour of recrystallized grain B.

The values of R are 0.9, 1.45 and 1.7 cms. The angle between R_1 and R_2 is 90° and 58° between R_1 and R_3. The ratios R_1/R_2 and R_1/R_3 are 0.62 and 0.529 respectively comparing the ratios with ratios of d values, possible indices are (111), $(0\bar{2}2)$ and $(1\bar{1}3)$. Angle between (111) and $(0\bar{2}2)$ is given by $\cos^{-1}(\frac{0}{\sqrt{3 \times 8}})$ i.e. 90° which is exactly equal to measured value. Angle between (111) and $(1\bar{1}3)$ is given by $\cos^{-1}(\frac{3}{\sqrt{3 \times 11}})$ i.e. 58.5^O which fit very well with the measured angle. The electron beam direction is $[2\bar{1}1]$.

E

This SAD is from strained region in neighbour of recrystallized grain B. The values of R are 0.87, 0.87 and 1. The angle between R_1 and R_2 is 110° and 55° between R_1 and R_3. Using ratio method planes were found to be (111), $(\bar{1}\bar{1}1)$ and (002) and the electron beam is $[1\bar{1}0]$. It should be noted that beam direction for this region is same as that for recrystallized grain. One more micrograph showing two recrystallized grains in neighbour is shown in Figure 4.7. Selected area diffraction patterns from three regions in the micrograph are pasted near to the corresponding regions i.e. two from the two different recrystallized grains and third from the strained region. Analysis of these SAD's gives the orientation relationship between these three regions.

SAD from upper recrystallized grain:

The 'R' values are 1.0, 1.0, 1.5 cms. The angles between R_1 and R_2 is 90° and 46.5^O between R_1 and R_3. The
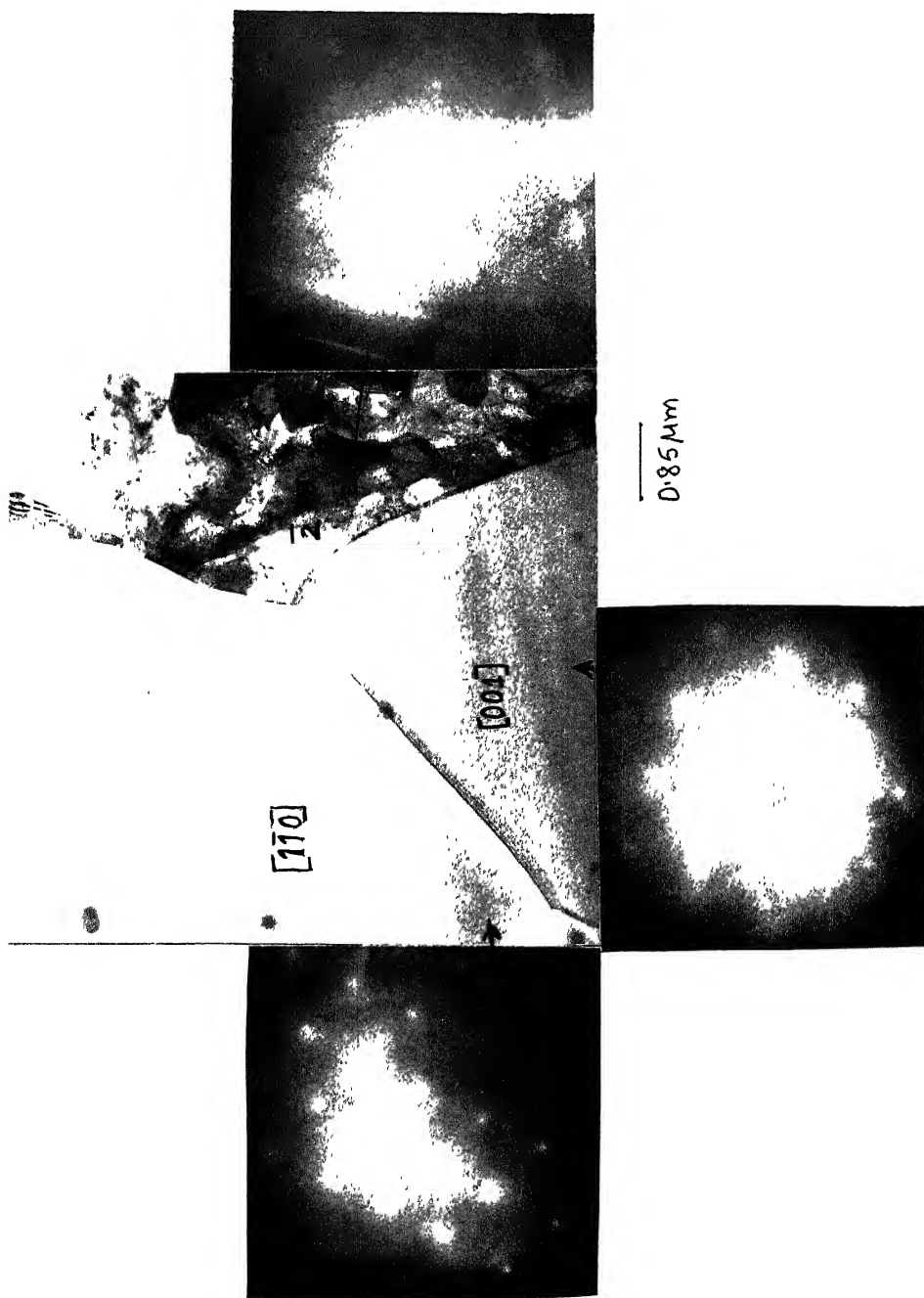
Fig. 4.7 (a) Recrystallized grain and deformed region in Al—Mg after two stage annealing, (b) Diffraction pattern from recrystallized grains and (c) Diffraction pattern from deformed region on right.

ratios R_1/R_2 and R_1/R_3 are 1.0 and 0.66 respectively. Comparing these ratios with d ratios, indices of possible planes are (200), (020) and (220). The angle between (200) and (020) is $\cos^{-1} 0$ i.e. 90° and the angle between 200 and 200 is $\cos^{-1} \dfrac{4}{\sqrt{3 2}}$ i.e. 45° which is quite close to measured value. The beam direction is [001].

SAD from lower recrystallized grain:

This diffraction pattern has been solved by ratio method as well as using Kikuchi lines. The 'R' values are 1.08, 1.1, 1.1 cms. The angle between R_1 and R_2 is 60° and 120° between R_1 and R_3. The planes evaluated are 313, $0\bar{2}4$ and $\bar{3}\bar{3}1$. The angle between 313 and $0\bar{2}4$ is given by $\cos^{-1} \dfrac{10}{\sqrt{19 \times 20}}$ i.e. 59.14^O which is quite close to measure angle. The angle between 313 and $\bar{3}\bar{3}1$ is $\cos^{-1} \dfrac{-9}{\sqrt{19 \times 19}}$ i.e. 118.27 which is nearly equal to the measured value. The beam direction is [$\bar{2}$33].

SAD from strained region:

The 'R' values are 0.86, 0.86 and 1.0 cms. The angles between R_1 and R_2 is 110° and 54° between R_1 and R_3. The ratios R_1/R_2 and R_1/R_3 are 1 and 0.86 respectively. The possible planes are 111 , 002 , $\bar{1}\bar{1}1$ and the beam direction is [$1\bar{1}0$].

So it shows the orientation of these three regions is different.

4.3 Differential Scanning Calorimetric Analysis of 7075 Aluminium Alloys:

4.3.1 Results:

DSC has been used to characterize the solid state reactions accompanying heating of the following tempers, (i) solution treated, (ii) solution treated and cold rolled (90 percent), (iii) T6, (iv) RRA and (v) T85. The steps involved in these heat treatments have already been explained in Chapter II (Table 2.1). The microstructure of (i) and (ii) consists of supersaturated solid solution (SSSS) and deformed SSSS. As pointed out earlier the matrix microstructure of the T6, RRA and T85 tempers of 7075 aluminium consists primarily of GP zones with a small concentration of semicoherent η' phase (Table 2.2) although the volume fraction of these two are different in these three tempers. DSC technique was used to characterize the solid state reactions accompanying the dissolution of the preexisting matrix precipitates as well as the formation of additional precipitates. The DSC curves i.e. differential heat capacity vs. temperature curves for these tempers are shown in Figures 4.8 to 4.13 at two different heating rates of 10°C/min and 15°C/min in most of cases. In these curves deviation from the horizontal are indicative of solid state reactions accompanying heating. The C_p values have been calculated by using relationship:

$$C_p = (\frac{60 \; E \; \Delta q_s}{H_R}) \; \frac{\Delta y}{m}$$

where
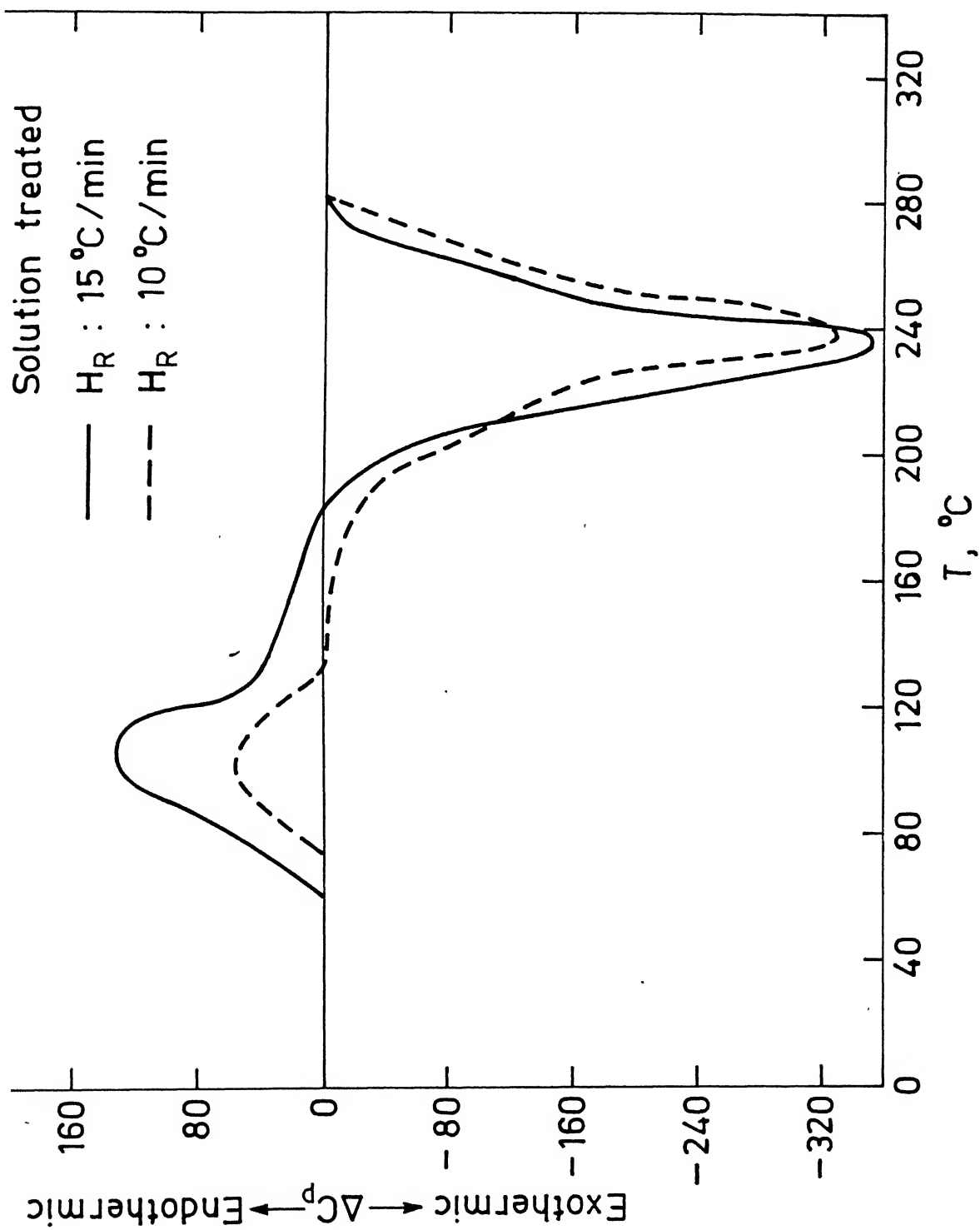
Fig. 4.8. Heat capacity changes accompanying solid state reactions in solution treated 7075 aluminium alloy
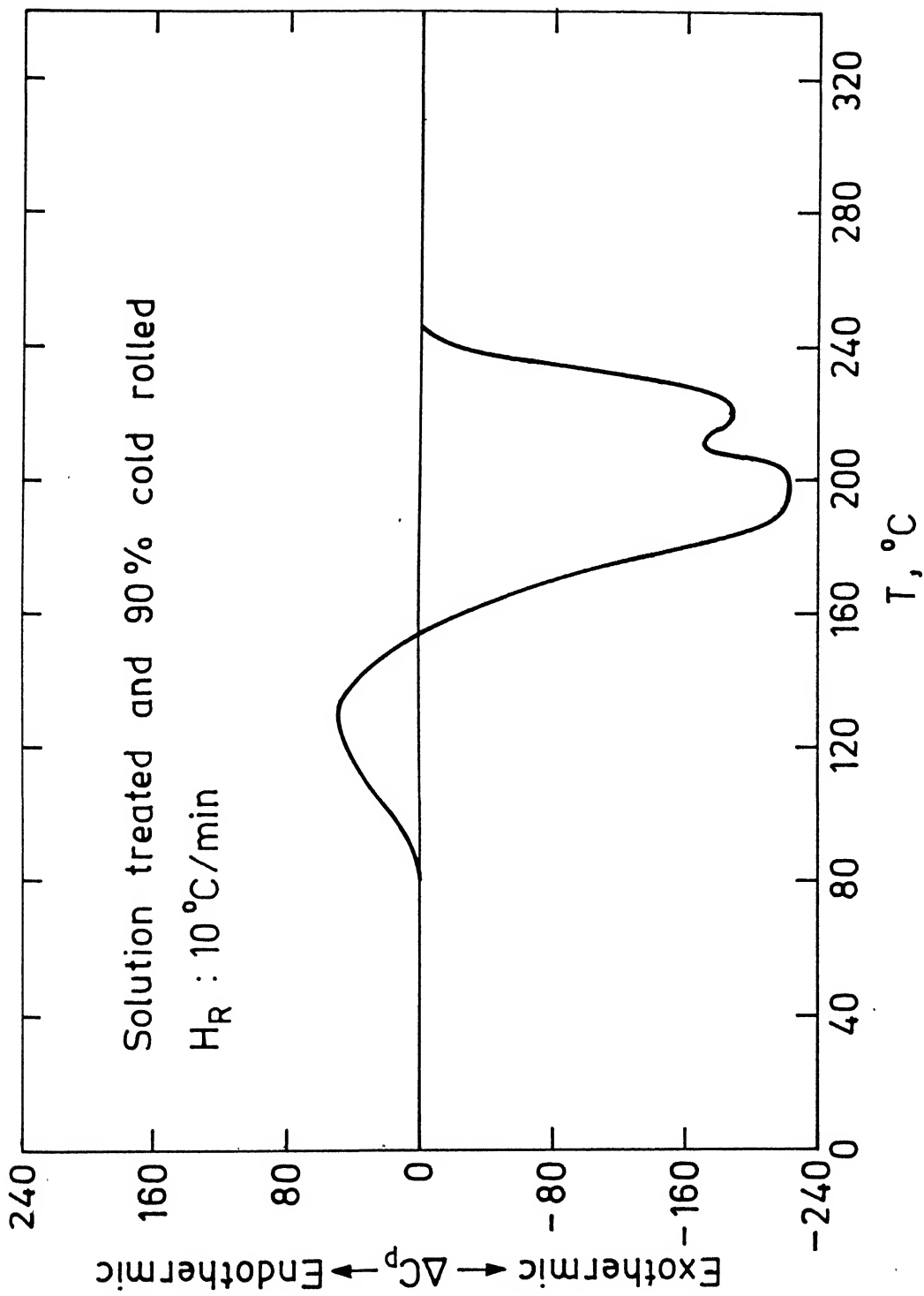
Fig. 4.9.   Heat capacity changes accompanying solid state reaction in solution treated and cold rolled 7075 aluminium alloy
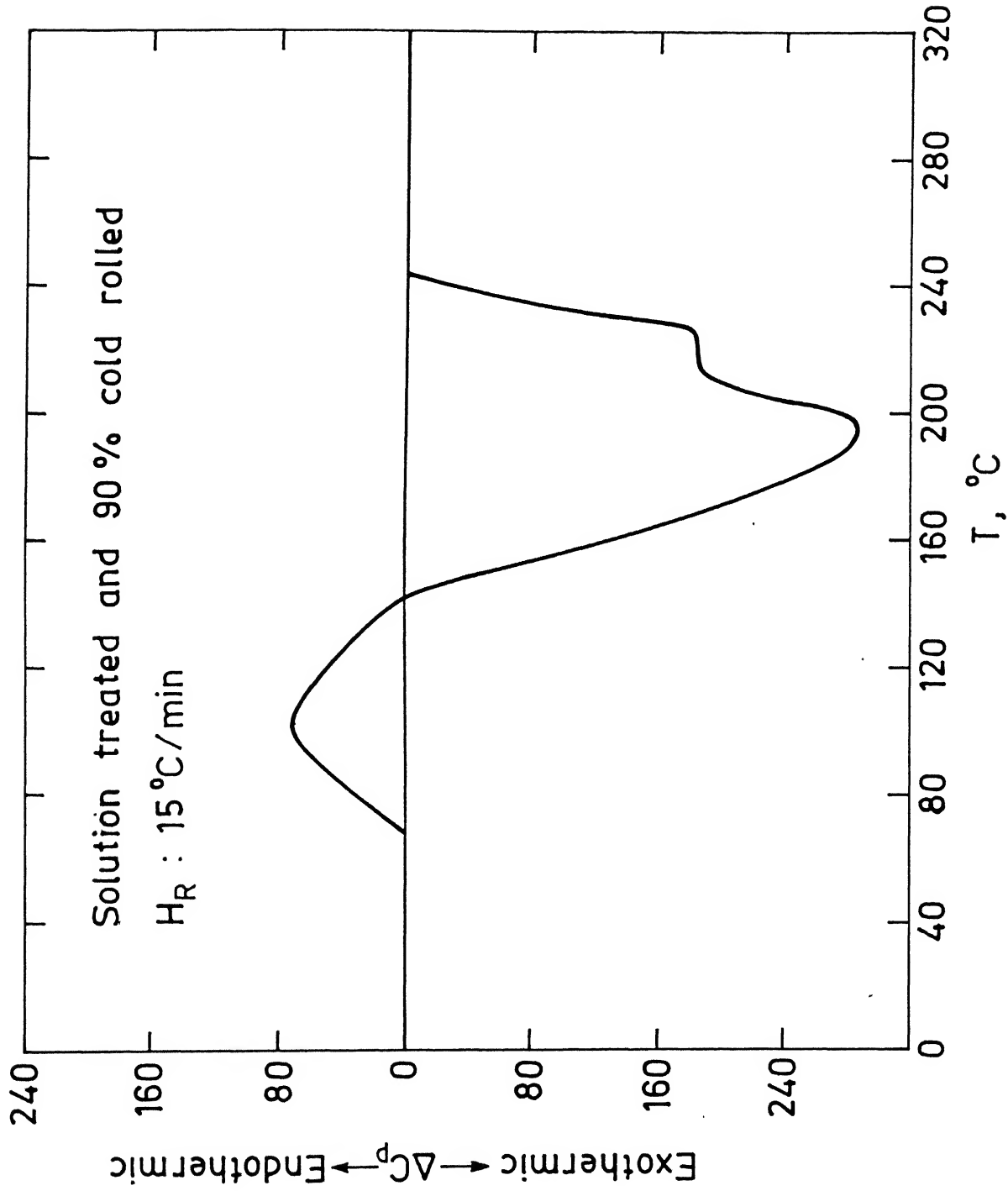
Fig. 4.10. Heat capacity changes accompanying solid state reactions in solution treated followed by cold rolling 7075 aluminium alloy
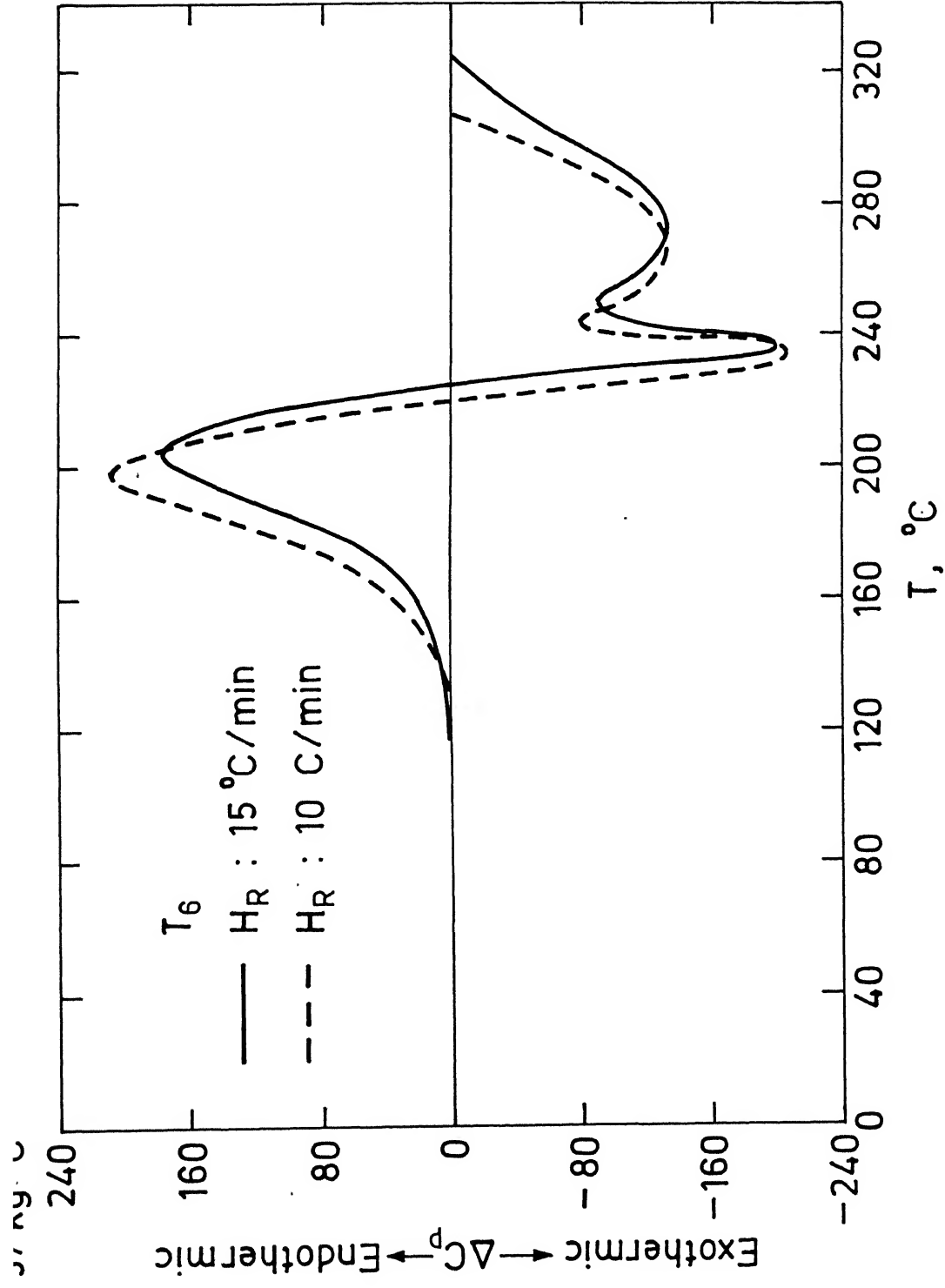
Fig. 4.11. Heat capacity changes accompanying solid state reactions in 7075 alloy after T_6 treatment
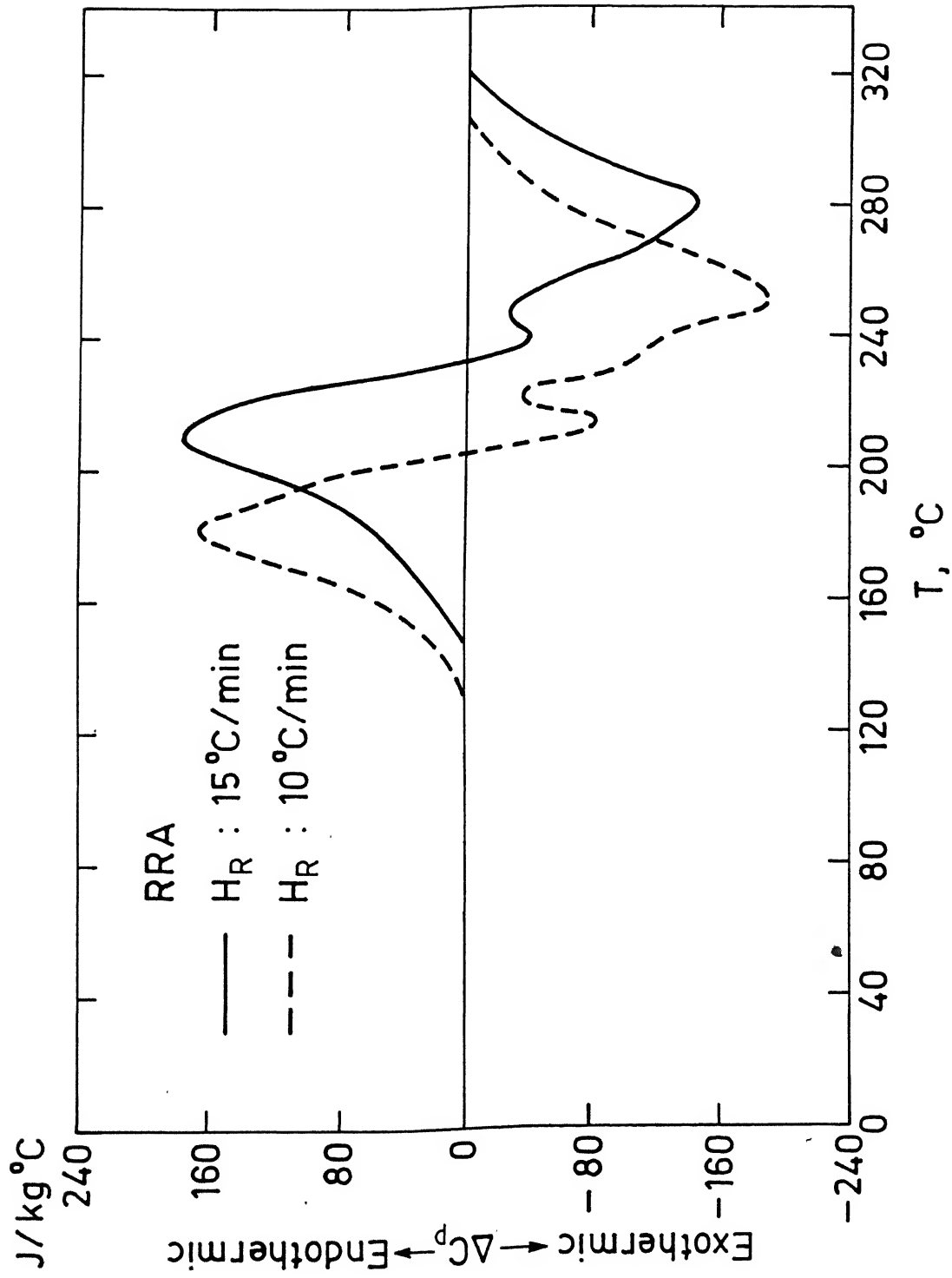
Fig. 4.12. Heat capacity changes accompanying solid state reactions in 7075 aluminium alloy after retrogression and reaging treatment
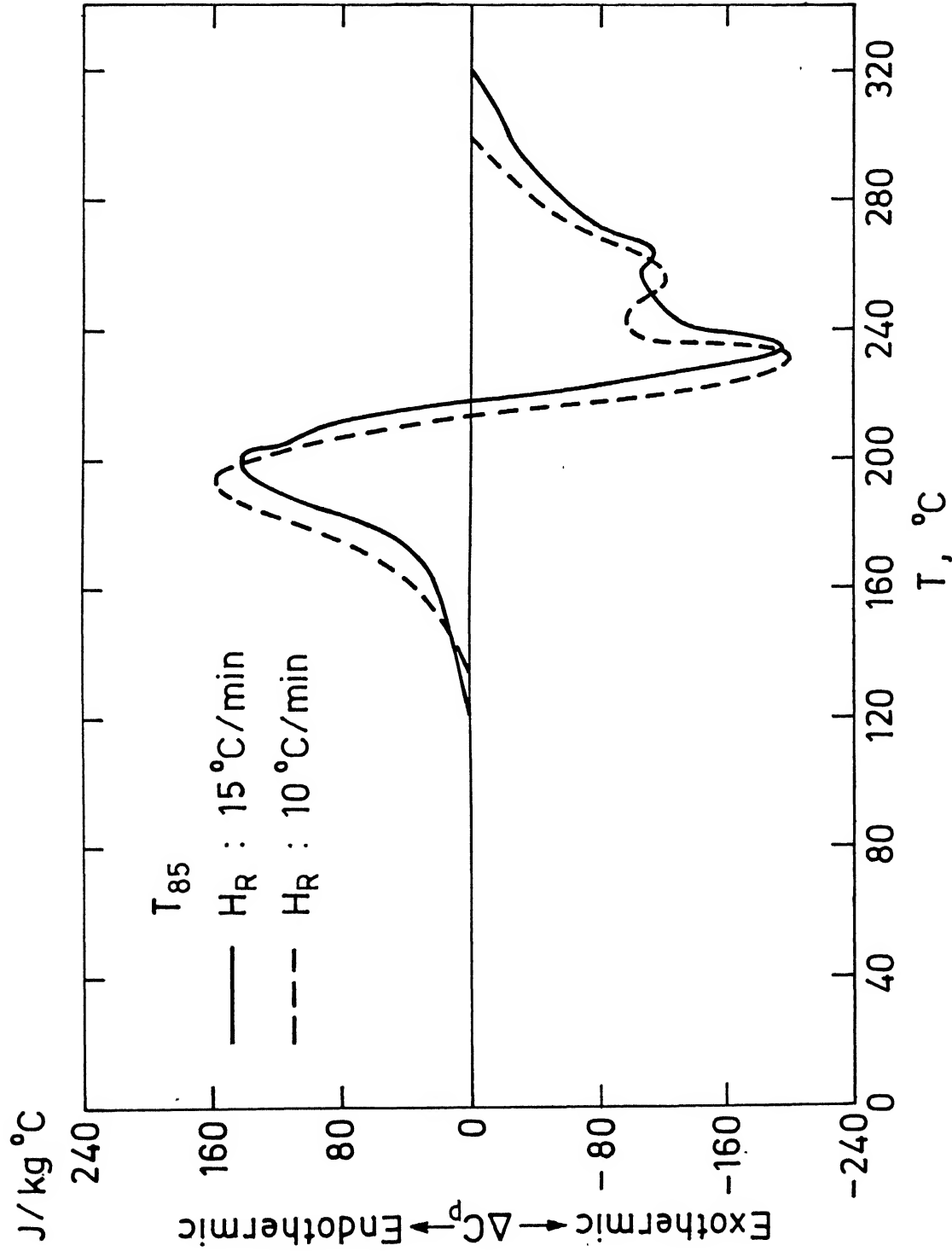
Fig. 4.13. Heat capacity changes accompanying solid state reations in 7075 aluminium alloy after T_{85} treatment
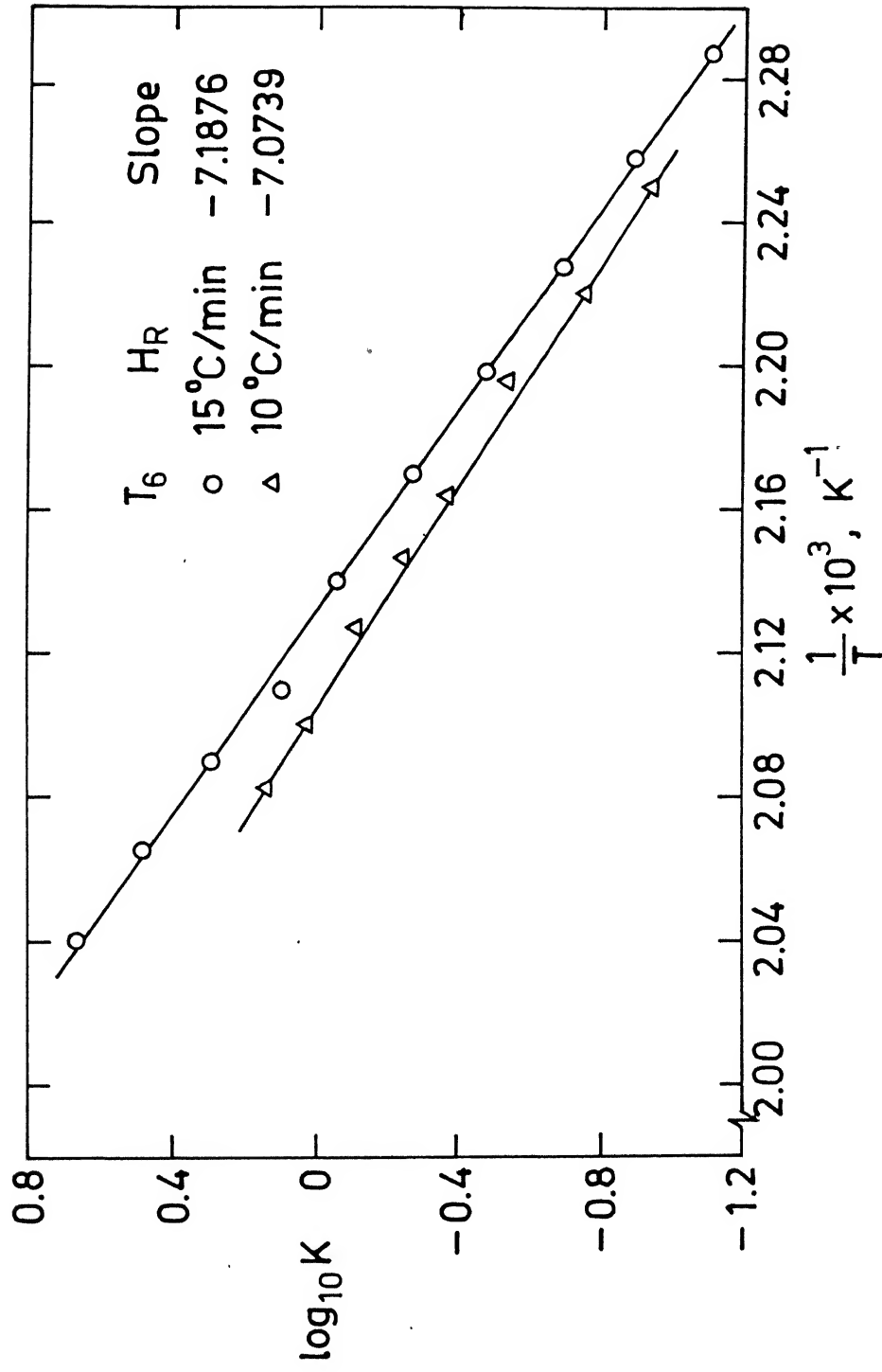
Fig. 4.14. $\log_{10} K$ vs $\frac{1}{T} \times 10^3$ plot for dissolution peak of T_6 temper of 7075 aluminium at heating rates $10°C/min$ and $15°C/min$
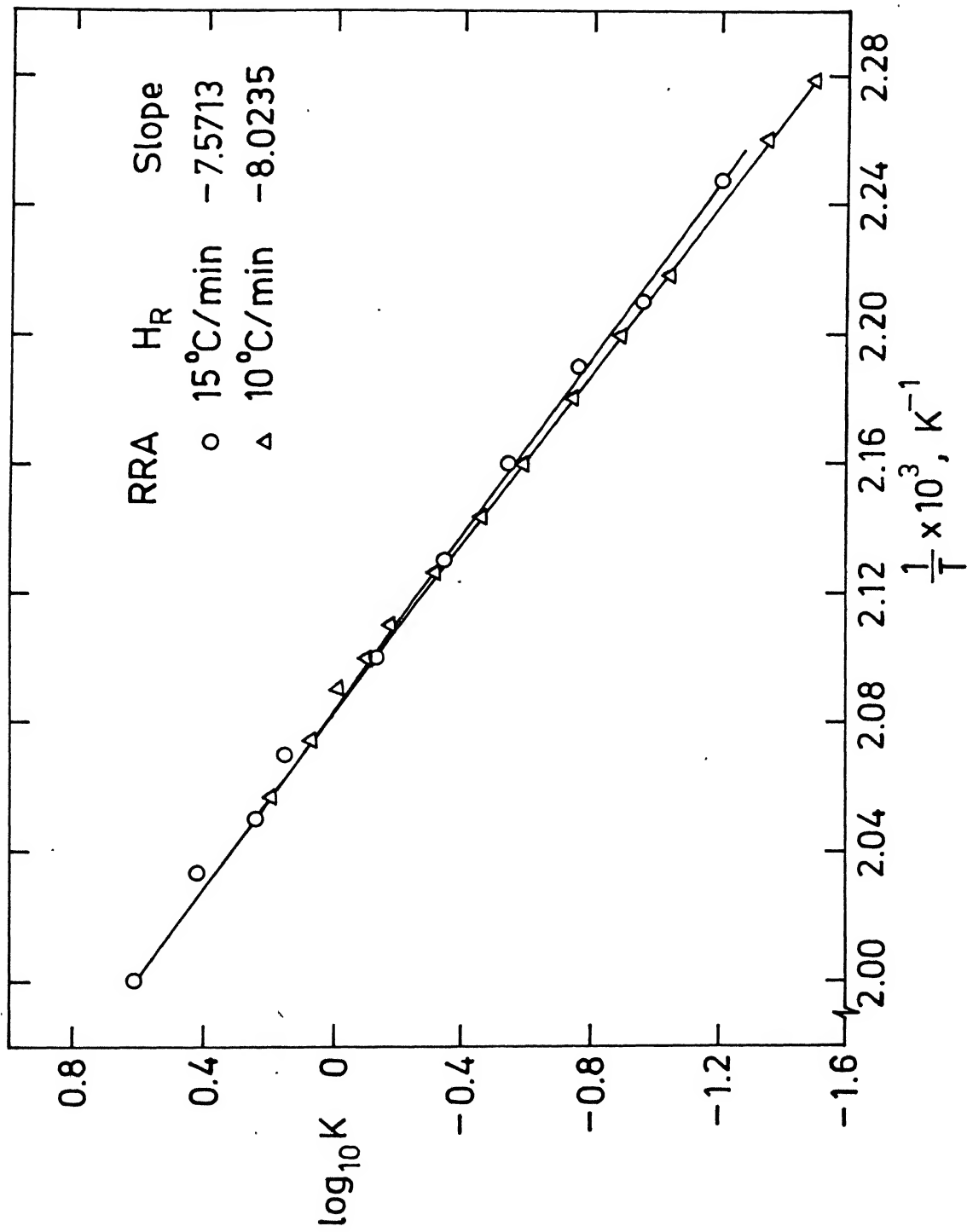
Fig. 4.15. $\log_{10} K$ vs $\frac{1}{T} \times 10^3$ plot for dissolution peak of RRA temper of 7075 aluminium at heating rates 10°C/m and 15°C/min
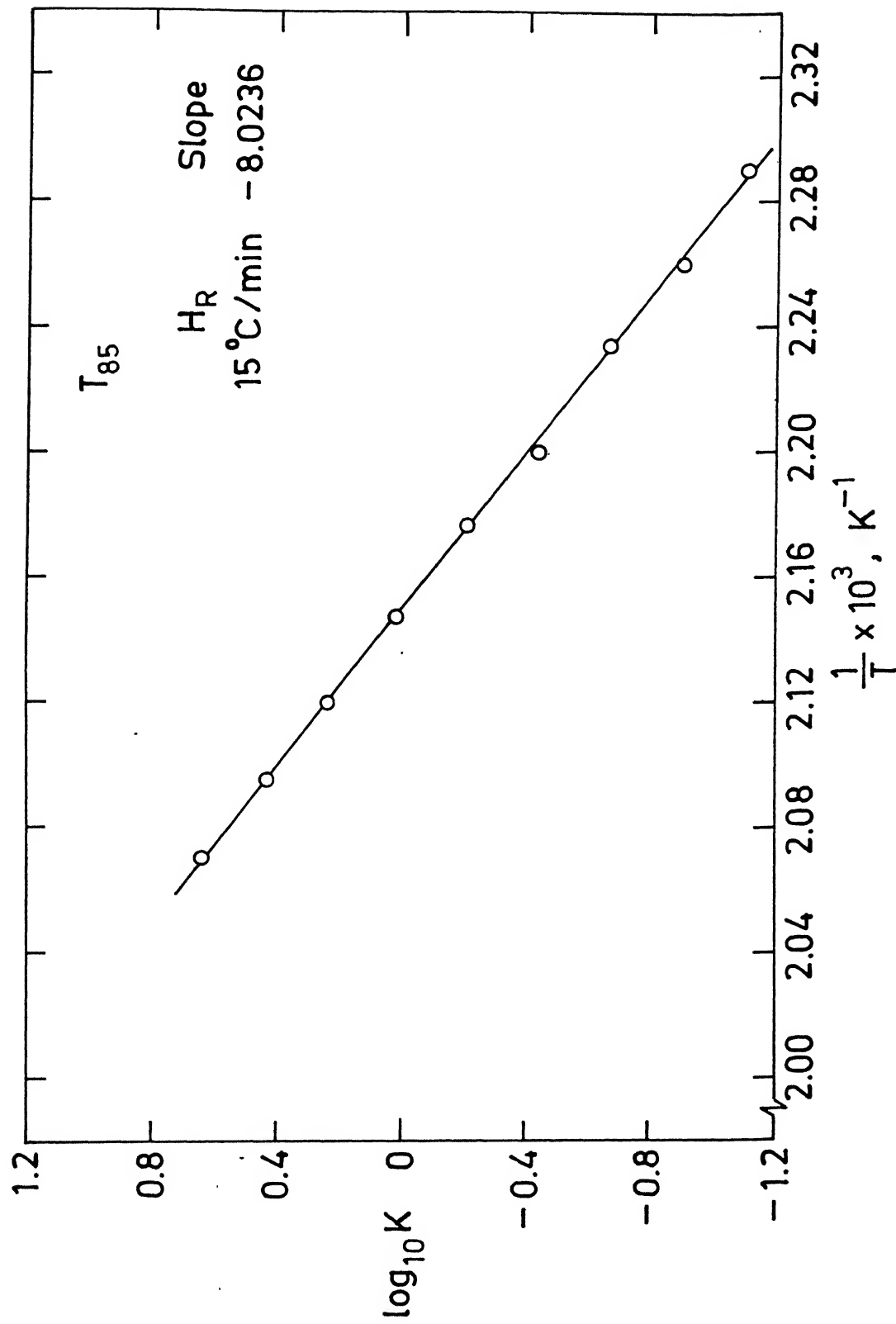
Fig. 4.16. $\log_{10}K$ vs $\frac{1}{T} \times 10^3$ plot for dissolution peak of T_{85} temper of 7075 aluminium at heating rate 15°C/min

Table 4.1: DSC characteristics of 7075 aluminium alloy

Temper	Q °C/min	Region	Nature	Temperature range of specific region °C	Temperature range chosen for kinetic analysis °C	Peak temperature T_p °C	ΔH_R J/kg	E_a kJ/mole	$\Delta S^{\ddagger}$ J/mole °K	$\Delta G^{\ddagger}$ kJ/mole
	1	2	3	4	5	6	7	8	9	10	11
Solution treated	10	I	Endoth-ermic	74–134	–	97	·1726±200	–	–	–
		II	Exoth-ermic	134–282	–	238	12800±1000	–	–	–
Solution treated	15	I	Endoth-ermic	60–183	–	104	3053	–	–	–
		II	Exoth-ermic	183–281	–	238	10549±710	–	–	–
Solution treated + cold rolled (90 percent)	10	I	Endoth-ermic	86–154	–	126	1968	–	–	–
		II	Exoth-ermic	154–244	–	(i) 198±2 (ii) 221	14602±730	–	–	–
Solution treated + cold rolled (90 percent)	15	I	Endoth-ermic	68–142	–	102	3961±200	–	–	–
		II	Exoth-ermic	142–242	–	(i) 196±2 (ii) 222	18805±969	–	–	–

Contd...

Table 4.1 (continued)

1	2	3	4	5	6	7		8	9	10	11
T6	10	I	Endoth-ermic	130–219	164–211		197	7464	135	–220	114
		II	Exoth-ermic	219–306	–	(i) 233 (ii) 262		9326±108	–	–	–
T6	15	I	Endoth-ermic	117–223	164–211		199	8974	137	–220	78
		II	Exoth-ermic	223–323	–	(i) 234 (ii) 274±2		9459	–	–	–
RRA	10	I	Endoth-ermic	152–222	166–217		203	5926±110	145	–233	119
		II	Exoth-ermic	222–299	–	(i) 226 (ii) 270±2		6706±2100	–	–	–
RRA	15	I	Endoth-ermic	147–231	172–224		210	6645±694	148	–227	119
		II	Exoth-ermic	231–322	–	(i) 240 (ii) 282		5095±790	–	–	–
T85	10	I	Endoth-ermic	136–214	–		194	6875±600	–	–	–
		II	Exoth-ermic	214–300	–	(i) 230 (ii) 254		8200±280	–	–	–
T85	15	I	Endoth-ermic	122–218	163–210		200	6683±594	154	–225	116
		II	Exoth-ermic	218–322	–	(i) 234 (ii) 264		8000±300	–	–	–

E   =   Cell calibration coefficient in mW/mV (dimension-
        less) (E = 204.7 μW/mV for all DSC runs).

Δq_s =   Y-axis range i.e. mV/cm (4 mV/cm in these cases)

H_R =   Heating rate ($^{\circ}$C/min)

Δy =   Height from the base line (cm)

m   =   Mass (mg).

The calibration coefficient was checked by using tin as the
standard. For this, DSC run was used at a heating rate 10°C/min.
Endothermic peak was observed at 232°C which is exactly equal
to melting point of tin. Heat of fusion, ΔH_f, of tin calcu-
lated from DSC curve. was compared with the theoretical value,
error in calculated value of ΔH_f has been taken care of by
correcting, E, the cell calibration constant. This corrected
value of cell calibration constant has been used for all the
experiments on 7.075 alloy. The differential heat capacity was
obtained by subtracting a background heat term from the
calorimetric data. The background heat term in the temperature
dependent heat capacity of aluminium rich solid solution and
the existing precipitates. It was established for each run by
considering the initial and final calorimetric measurements
during which thermal equilibrium was approached as well as
the specific heat measured over temperature ranges whereas no
reaction took place.

Two types of regions observed in DSC curves (i) endo-
thermic and (ii) exothermic were analysed to characterize the
reaction temperature and enthalpy corresponding to specific
temperature range. Kinetics of the dissolution reactions in
T6, RRA and T85 tempers have been evaluated.

The peak temperature, T_p, for a specific endotherm or exotherm is a measure of the temperature at which the reaction is occurring at a maximum rate. For example, T_p for endotherm gives the temperature at which dissolution reaction is occurring at a maximum rate.

The area of specific endothermic or exothermic region of ΔC_p vs. T curves corresponds to the enthalpy associated with the reaction occurring over the indicated temperature range. For example, area of the endotherm for each temper is a measure of the heat of reaction associated with precipitate dissolution. For a specific precipitate this heat, ΔH_R, is proportional to the volume fraction of the precipitate undergoing dissolution. This is shown in the following equation

$$\Delta H_R = \frac{\Delta H_p}{M_p} \frac{\rho_p}{\rho_s} V_f$$

The kinetics associated with dissolution of precipitates for T6, T85 and RRA have also been evaluated. If the dissolution reaction is considered to be of first order, the rate of reaction is proportional to the concentration of the reacting species, i.e.,

$$-\frac{dc}{dt} = K_r C$$

where

$\quad K_r$ = specific reaction rate constant, and

$\quad C$ = reactant concentration.

For DSC, the rate of reaction is monitored by the rate of heat flow. The concentration of reactant remaining at any

time, t, is represented by the total area, A (under endotherm) minus the area under the peak to time t, a_t i.e., $C = A - a_t$. Therefore

$$\frac{dH}{dt} = K_r(A - a_t)$$

Substituting $dH = \Delta C_p dT$ and solving for the reaction rate yields

$$K_r = Q \frac{\Delta C_p}{(A - a_t)} \qquad (4.1)$$

where

$$Q = \frac{dT}{dt} \text{ i.e., constant heating rate.}$$

Using this relationship (4.1), value of K_r as a function of temperature were obtained by computer programmed stepwise integration of the dissolution peak (Trepezoidal rule). The $\log_{10} K_r$ vs. $\frac{1}{T} \times 10^3$ are plotted for T6, RRA and T85 tempers and shown in Figures 4.14, 4.15 and 4.16 respectively. The slope of this curve, m, is used to calculate activation energy using following relationship:

$$m = -\frac{E_a}{2.303 \cdot R}$$

where

E_a = activation energy (kJ/mole)

R = gas constant (kJ/mole).

Absolute reaction rate theory is applied to calculate activation entropy of dissolution reactions for each temper. The formula used is:

$$K_r = (kT/h) \, e^{\Delta S^{\ddagger}/R} \cdot e^{-\Delta H_R/RT}$$

where

K_r = rate constant for reaction

k = Boltzmann constant = 1.38×10^{-23} J/K^{-1}

h = Planck's constant = 6.626×10^{-34} J-sec

T = temperature (degree Kelvin)

$\Delta S^{\ddagger}$ = change in entropy

ΔH_R = heat of reaction

R = gas constant = 8.314 J mole^{-1} K^{-1}.

The activation entropy value has been used to compare the relative stability of preexisting matrix precipitates in the three tempers i.e. T6, RRA and T85.

Free energy of activation, $\Delta G^{\ddagger}$, has been evaluated using relationship:

$$\Delta G^{\ddagger} = \Delta H - T \Delta S^{\ddagger} \quad \text{or} \quad \Delta G = E_a - T(R + \Delta S^{\ddagger})$$

The results of DSC curves analysis i.e. regions observed, temperature range over which a specific region i.e. endotherm or exotherm is observed, temperature range chosen for kinetic analysis, peak temperature, enthalpy, activation energy, activation entropy and free energy of activation corresponding to a specific region have been tabulated in most of the tempers in Table 4.1.

4.2.2 Discussion:

As shown in Figure 4.8, DSC curves for solution treated (S.T) samples at 10°C/min and 15°C/min consist of

endotherms at lower tempers which corresponds to dissolution of GP zones that possibly formed during natural ageing for a few days (~1 week). Since the time of natural ageing is different for different samples, different amount of GP zones are expected to form. This came true on comparing the heat of dissolution reactions, ΔH_R, for different samples. An exotherm at higher temperature is due to precipitation of GP zones, intermediate η' phase and equilibrium η phase. The peak of temperature at both heating rates ($238^{\circ}C$) indicates that precipitation of η' and η would be dominating reactions.

For solution treated and 90 percent cold rolled (S.T + C.R) sample, cold rolling was done immediately after quenching so that the GP zones during natural ageing would form in deformed matrix. Endotherms observed at lower temperature are due to dissolution of these GP zones. On comparing the characteristics of this DSC endotherm at $10^{\circ}C/min$ with that for S.T sample at same heating rate, it is seen that ΔH_R values are quite comparable for the two indicating the same volume fraction of GP zones dissolving. Difference in their peak temperatures (Table 4.1) and shape of curves (Figures 4.8 and 4.9) implies that dissolution of GP zones is faster in S.T than in S.T + C.R sample. Exothermic regions for solution treated and cold rolled samples show two maxima (Figures 4.9 and 4.10) at temperatures (Table 4.1). The first minima can be due to recrystallization and the second due to precipitation of η' and η. The temperature of second maxima is lower than that of single maxima in S.T sample. Because of presence of dislocations and other defect structure, the precipitation of

η' and η gets accelerated which is responsible for lower value of temperature of second maxima. ΔH_R values for these exotherms are higher than that for S.T samples. There can be two reasons for these differences: (i) due to presence of dislocations etc. more of η' and η precipitate in deformed sample and (ii) additional ΔH_R possibly due to recrystallization.

DSC curves for T6 temper are shown in Figure 4.11 and their characteristics are tabulated in Table 4.1. Endotherms observed for both the heating rates 10°C/min and 15°C/min correspond primarily to the dissolution of GP zones. η' present in matrix would also be expected to dissolve. Furthermore, limited formation and growth of η' phase occurs within this region which affects the endotherm. Two exothermic peaks have been observed over a single range of temperature. Over this whole range, the expected reactions are η' formation, η formation and η growth. The temperature range containing the first maximum, $T < 250^\circ$C corresponds to the formation of η from pre-existing η'. Over the temperature range of second maximum, $T > 250^\circ$C, growth of η particles takes place exclusively. The existence of the doublet therefore, is indicative of two separate reaction ranges within second exothermic region. Comparing the endothermic region of T6 with that of S.T sample. The peak temperature for S.T samples ($\approx 97^\circ$C) is much less than that for T6 sample ($\approx 197^\circ$C) indicating that GP zones in T6 are much more stable than those in S.T samples. Higher values of ΔH_R for T6 temper than that for S.T samples shows the amount of GP zones in T6 is approximately 7 times more than that in S.T samples which are naturally aged for 1 week. The maxima of

exothermic region of S.T sample is approximately the same as first maxima of T6 sample. But heat of reaction, ΔH_R, for S.T sample is larger than that for T6 sample which indicates the large volume of precipitates forming in S.T sample which is expected also due to higher supersaturation in S.T sample.

For the retrogression and reageing treated 7075 aluminium, also two regions are observed (Figure 4.12). It has already been explained in detail (Chapter II) that RRA treated alloy contains a volume fraction of η' which is greater than that in T6 treated alloy. Also the volume fraction of GP zones is less. The start and end of dissolution curve, as compared to that of T6 treated sample, has shifted towards right. In addition a shift of peak temperature towards higher temperature indicates that the preexisting precipitates in RRA treated sample are relatively more stable than in T6 treated. Two exothermic peaks occur over a same temperature range of reaction. The comparison of these two peak temperatures with those in exothermic region of DSC curve for T6 shows that first peak in RRA should also correspond to precipitation of η' and η while the second peak to growth of η. Area under the first peak is very small in RRA temper which could be due to less amount of η' precipitating because preexisting η' volume fraction in RRA is more than that in T6 matrix microstructure (Table 2.3). Second maxima in this case is also due to growth of η.

The DSC curve for T85 is similar to that for T6 temper. The temperature range of reaction, their corresponding peak temperatures are approximately same (Table 4.1). ΔH_R value for

endotherm is slightly less for dissolution of preexisting
precipitates in T85 than in T6 which shows the volume fraction
dissolving GP zones in T85 is less than that in T6. The
exotherms and their characteristic are similar except the area
under second maxima which is slightly less than that in T6
indicating that growth of η is restricted in T85 temper. We
have seen that in the three temper T6, RRA, T85, region I i.e.
endotherm corresponds to GP zones and η' dissolution and
exothermic region corresponds to η' and η formation and η
growth. With this understanding of predominant microstructural
changes associated with specific temperature regions, the
significance and kinetic data obtained from DSC curves can be
discussed now.

The kinetics associated with the dissolution during
endothermic region can be characterized by specific values of
activation energy and activation entropy that are base on the
model of absolute reaction rate theory. These values are
listed in Table 4.1. The activation energy is minimum for T85
temper, intermediate for RRA, and minimum for T6 temper. The
entropy change associated with the formation of the activated
complex is highest for RRA temper than for T85 and smallest
for T6 temper. The highest negative activation entropy for
preexisting precipitates of RRA temper being indicative of
having lowest activation sight probability. The results show
that the preexisting precipitates are most stable in RRA
temper and intermediately stable in T85 and least stable in
T6 temper. If the appropriate kinetic barrier to dissolution

is considered i.e. free energy of activation, $\Delta G^{\ddagger}$, it is
found to be maximum for RRA temper, intermediate for T85
and maximum for T6 temper. These result show that the disso-
lution kinetics of the matrix preexisting precipitates is
primarily influenced by the entropy rather than the activation
energy.

CHAPTER V

CONCLUSIONS

The following conclusions can be drawn on the basis
of results and discussion presented in Chapter IV.

1.   TEM studies on Al-Mg alloys shows that these alloys
      show extensive macroscopic shear bands after cold
      rolling (ε_T = 1.7).

2.   After two stage recrystallization: (i) 243°C for
      2 min and (ii) 275°C for 2 min a number of transforma-
      tion observed are: (a) decrease in density of shear
      bands, (b) recovery at some places showing formation
      of subgrains, (c) nucleation of recrystallized grains
      at original high angle grain boundary by subgrain
      coalescence, (d) nucleation of recrystallized grain at
      shear bands and (e) a few fully recrystallized grains.
      Thus we can conclude that shear band and original high
      angle grain boundaries act as recrystallization sites.

3.   The distribution of orientation among strained,
      recovered and recrystallized region have been evalu-
      ated from the selected area diffraction patterns.

4.   Differential scanning calorimetric analysis of 7075
      aluminium alloy has been used to study the solid state
      reactions accompanying various tempers like solution
      treated, solution treated plus 90 percent cold rolled,
      T6, RRA i.e. retrogression and reaged, T85 in the

temperature range 30 to 300°C. These reactions have been elucidated and expressed in terms of thermodynamic and kinetic parameters.

5. The dissolution parameters (peak temperature, dissolution enthalpy, activation energy, and activation entropy) for each phase are distinguishable and useful for a rapid characterization of the matrix microstructure of 7075 aluminium alloys.

6. Recrystallization in solution treated and 90 percent cold rolled temper has also been studied.

7. The peak temperature of dissolution peaks can be used to compare the relative stability of preexisting precipitates in different tempers.

8. Enthalpy i.e. area under the dissolution peak is directly proportional to the volume fraction of precipitates dissolving.

9. The relative stability of preexisting precipitates in T6, T85 and RRA tempers is related primarily to the activation entropy. The preexisting precipitates are most stable in RRA temper and intermediately stable in T85 and least stable in T6 temper.

REFERENCES

1. L.F. Mondolfo, ''Aluminium Alloys : Structure and Properties'', Butterworths, London (1976), P. 312.

2. L.F. Mondolfo, ''Aluminium Alloys : Structure and Properties'', Butterworths, London (1976), P.313.

3. D.J.Lloyd, Ed. F. Butryn and Moy Ryvola, Deformation Morphology in cold rolled Al-Mg alloys, Microstructural Science, Vol. 10, PP. 373-84.

4. L.F. Mondolfo, ''Aluminium alloy : Structure and Properties'', Butterworths London (1976).

5. D.J. Lloyd, ''The influence of particles and deformation structu on recrystallization''.

6. J. Polmear, ''Light Alloys : Metallurgy of the light Metals'', Edward Arnold, London (1981), P. 15.

7. R. Ayer, J.Y. Koo, J.W. Steeds and B.K. Park, ''Microanalytical study of the heterogeneous phases in Commercial Al-Zn-Mg-cu alloy Met. Trans A., (1985) Vol. 16A, P. 1925.

8. P.N.Adler, R. Deiasi, and G. Geschwind, ''Influence of microstruc on the mechanical properties and stress corrosion susceptibility of 7075 alloy'', Met. Trans, (1972) Vol. 3, PP 3191-3200.

9. S.E. Naess, Scripta Met., (1969), Vol. 3, P. 179.

10. G. Thomas, and J. Nutting, J. Inst. Metals, (1959-60), Vol. 88, P

11. Embury, J. D. and Nicholson, R.B., Acta Met., (1965) Vol. 13, P.4

12. L.F. Mondolfo, N.A. Gjostein, and D.W. Levinson, AIME Trans., (19 Vol. 206, P. 1378.

13. J. Gjonnes, and C.J. Simensen, Acta Met, (1970) Vol. 18, P. 881.

14. Schmalzried, H. and Gerold, V., Z. Metallk., 1958, Vol. 49, P.291.

15. J.A. Wert, N.E. Paton, C.H. Hamilton and M.W. Mahoney, ''Grain Refinement in 7075 aluminium by thermomechanical processing'' Met. Trans. (1981) Vol. 12A, P.1267.

16. A.S.Keh, Direct observation of lattice defects in crystals, Interscience, New York, (1962) P.213.

17. D.H. Warrington, Proc. European regional Conf. On Electron Microscopy , Delft (1961) P.354.

18. Bellier, S.P. and Doherty, R.D. Acta Met. (1977)., 25, PP521-58.

19. Inokuti, Y. and Doherty, R.D, Texture, (1977), 2, PP 143-168.

20. Inokuti, Y. and Doherty, R.D, Acta Met., (1978) 26, PP 61-80.

21. Kreisler, A. and Doherty, R.D, Metal Science , (1978), 12, PP551-560.

22. Humpnreys, F.J, ''The nucleation of recrystallization at second phase particles in deformed Aluminium'', Acta Met., (1977) 25, PP. 1323-44.

23. Herbst, P. and Huber, J., ''Orientation of recrystallization nuclei in a deformed AlMgSi1-alloy'', Texture of materials. Edited by G. Gottstein and K. Lucke (Springer-Verlag, Berlin) 1, PP.453-464.

24. Klein, H.P., Z. Metallkude., (1970), 61, PP564-72.

25. Hornbogen, E. and Koster, U, ''Recrystallization in two-phase alloys In . Recrystallization of metallic materials , Edited by F.Haessner, PP. 159-95.

26. Lea, C., Brett, S.J. and Doherty, R.D., Scripta Met., (1979), 15, PP 45-50.

27. R.W. Cahn, ''Recrystallization, Grain Growth and Textures, ed. H. Margolin, American Society of metals, Clereland, Ohio, (1966) P.99.

28. R.D.Doherty, Met. Science J., 8(1974), P.132.

30. Beck, P.A., J. Appl. Phys., 2o(1948), P.633.

31. HU,H., Electron Microscopy and strength of crystals, ed. G. Thomas and J. Washburn, Interscience, New York, (1953), P. 546.

32. Hu, H., Recovery and Recrystallization in Metals, ed. L. Himmel, Intersciences, New York, (1963), P. 311.

33. Li, S.C.M., J. Appl. Phys., (1962), Vol. 33, PP2958-65.

34. Doherty, R.D., Recrystallization of metallic materials, 2nd Ed. F. Haessner, Riederer-Verlag Stuttgart, PP.23-62.

35. Adcock, J., J. Inst. Metals (1922) Vol.23, PP 73-92.

36. Grewen, J., Noda, T. and Sauer, D., Metallkunde (1977), 68, PP.260-65.

37. Duggan, B.J., Hatherly, M., Hutchinson, W.B. and Wakefield, P.T., Metal Science (1978) Vol. 12, PP343-51.

38. Noda, T., Plege, B. and Grewen, J., Texture of materials (1978) Ed. G.Gottstein and K. Lucke, Springer Verlag Berlin, PP.443-49.

39. Huber, J. and Hatherly, M., Metal Science (1979), Vol.13, PP665-69.

4o. Humphreys, F.J. Acta Met., (1977) Vol. 25, PP1323-44.

41. Jones, A.R., Ralph, B. and Hansen, N., Metal Science (1979) Vol.13, PP .149-54.

42. P.N.Adler, R.Deiasi, and G.Geschwind, ''Influence of microstructure on the mechanical properties and 'stress corrosion susceptibility of 7o75 alloy'', Met. Trans., (1972) Vol. 3, PP. 3191-3200.

43. N.C.Danh, K. Rajan, and W.Wallace, A TEM Study of microstructural changes during retrogression and reaging in 7o75 aluminium, Met. Trans.A, (1985) Vol. 14A, PP 1843-49.

44. Hatch, ''Aluminium : Properties and physical Metallurgy'', ASM, (1983).

45. R.Deiasi and P.N. Adler, Met. Trans. A, (1977) Vol. 8A, PP1177-8

46. H.Inoue, T.Sato, Y.Kojima, and T.Takahashi : Met. Trans. A, (1981) Vol. 12A, PP.1429-34.

47. J.Gjonnes and Chr. J. Simensen : Acta Metall., (1970) Vol. 18, PP.881-90.

48. N.Ryum : Z. Metallkde., (1975) Vol. 66, PP.338-43.

49. I.Kovacs, et al. Acta Metall., (1980), Vol. 28, PP.1621-31.

50. J.M.Howe, Met. Trans. A, (1986) Vol. 17A, PP.593-6o5.

51. BD.S. Thompson : Thermal Analvsis, Academic Press, New York, NY, (1969) Vol.2, PP.1147-70.

52. K.Hirano and H. Iwasaki : Trans. Japan Inst. Metals, (1964), Vol. PP.162-70.

53. J.M.Papazian : Met Trans. A, (1981), Vol. 12A, PP.269-69.

54. J.M.Howe : Metallagraphy, (1983), Vol. 16, PP.275-86.

55. R.Nozato and S. Ishihara, Trans. Japan Inst. Metals, (1980), Vol. 21(3), PP.580-85.

56. K.Osamura and T.Ogura Met. Trans. A, (1984) Vol. 15A, PP.835-42.

57. H.Sizuki, M.Hanno, Y.Shiraishi and K. Hanawa, J.Japan Inst. Light metals, (1979) Vol. 29(12), PP.575-81.

58. J.Hajdu, L.Kertesz, CS. Lenart, and E.Nagy: Cryst. Lattice Defects, (1974), Vol. 5, PP.177-88.

59. L.Kertesz, Cs. Lenart, and M.Kovacs-Treer:Crys. Lattice Defects, (1979), Vol. 8, PP.177-88.

60. L.Kertesz, Cs Lenart, and M. Kovacs. Treer: Crys. Lattice Defects (1979), Vol. 8, PP99-1o4.

61. L.Kertesz, M.Koracs-Treer, and J. Kollar: Cryst. Lattice Defects, (1979) Vol. 8, PP 149-52.

62. C.Gracia Cordovilla and E. Louis: Scripta Met., (1984) Vol. 18, PP 291-94.

63. K.Asana and K.Hirano: Trans. Japan Inst. Metals, (1968) Vol.9, PP.24-34.

64. W.Lacon, H.P. Degischer, Zahra and Zahra, Scripta Met., (1980) Vol. 14, PP.253-54.

65. R.J.Deiasi and P.N.Adler, Met. Trans. A, (1977), Vol.8A PP1177-83.

66. P.N.Adler and R.J.Deiasi Met. Trans A, (1977) Vol.8A, PP.1185-90.

67. J.M.Papazian. Mater. Sci. and Eng. (1981) Vol. 51, PP223-30.

68. J.M.Papazian, R.J.Deiasi and P.N.Ad ler. Metal Trans A, (1980) Vol. 11A, PP135-40.

ME-1980-M-VER-REC.